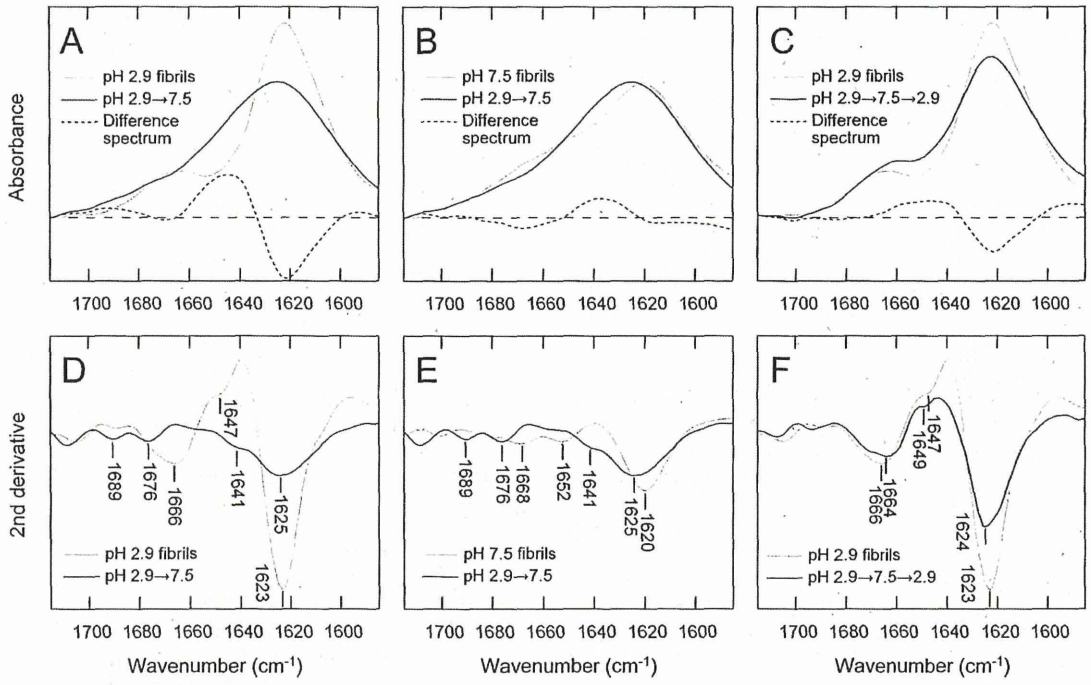

Figure 5. Conformation of H2 fibrils monitored by FT-IR spectra. (A)–(C) FT-IR absorption spectra of the fibrils before (gray solid line) and after (solid line) pH-jumps, and difference FT-IR spectra, subtracting the spectra before pH-jumps from those after pH-jumps (dotted line). (D)–(F) Secondary derivatives of FT-IR absorption spectra (A)–(C), respectively. Several β-sheet components are evident at 1620–1641 cm^{-1}, in addition to random conformations at 1647–1652 cm^{-1} and turn/loop conformations at 1664–1689 cm^{-1}.

(Figure 2K, gray), consisted of a large number of protofilaments, were observed (Figure 2G,H). Thus, pH 7.5-like fibrils (Figure 2K, gray) were much thicker than pH 2.9 fibrils before the pH-jump (Figure 2I, black). It is considered that the neutralization of electric repulsion between fibrils induces the assembly of fibrils. In fact, in the pH-jump to 7.5, the conformational change predominantly occurred along with the lateral association of the fibrils. Meanwhile, although the pH 2.9 fibrils consisted of several protofilaments (Figure 2A,D), the rotational symmetry axis[36] was unclear, and these fibrils often curved. The torsion of these fibrils was not recurrent. On the other hand, after the pH-jump from 2.9 to 7.5, protofilaments were fully assembled in pH 7.5-like fibrils (Figure 2H), but none of pH 2.9 fibrils and pH 7.5-like fibrils appears to associate with a rotational symmetry.

Double pH-Jump Experiments of H2 Amyloid Fibrils. The folding reaction of small-sized globular proteins is generally considered to be reversible at low protein concentrations.[37] Although a small number of reversible conformational or morphological changes of amyloid fibrils have been reported,[38,39] the mechanism of these reactions remains unknown. To investigate the reversibility of the conformational change of preformed H2 fibrils, a double pH-jump, pH 2.9 → 7.5 → 2.9, was performed using preformed by diluting 2.5-fold with buffers containing the same concentration of salt at every step. Intriguingly, pH 7.5-like fibrils with a minimum at 218 nm at pH 7.5 reverted to fibrils very similar to pH 2.9 fibrils, with an immensely large minimum at 207 nm at pH 2.9 (Figure 3A). These conformational changes were almost completed within the dead time of the manual pH-jump, 30 s (Figure 3A, inset). Next, the reversibility of pH 2.9 fibrils was investigated as a function of incubation time at pH 7.5. Efficiency gradually decreased as incubation time at pH 7.5 increased (Figure 3B,C). Although 93% of the pH 7.5-like fibrils reverted to pH 2.9 fibrils after 1 min of incubation at pH 7.5 (Figure 3C), after 72 h of incubation, approximately 50% of the pH 7.5-like fibrils had reverted to pH 2.9 fibrils. This irreversibility can be explained by the formation of an irreversible aggregate during the incubation at pH 7.5.

EM observations showed that, after the double pH-jump experiment with 1 min of incubation at pH 7.5, we observed two types of amyloid fibrils, one were thin fibrils (Figure 4A) and the other were thick fibrils consisted of a large number of protofilaments (Figure 4D). After 10 min of incubation at pH 7.5, we also observed thin (Figure 4B) and thick (Figure 4E) fibrils. After 3 h, we observed thin (Figure 4C) and thick (Figure 4C, arrow) fibrils. Although the population of these heterogeneous fibrils was unknown from EM measurements correctly, the fraction of fully recovered fibrils, which was obtained from CD measurements, decreased as the incubation time at pH 7.5 increased (Figure 3C).

Subsequently, light scattering measurements were performed to monitor the overall extent of fibril assembly (Figure 4F, left ordinate). After the pH-jump from 2.9 to 7.5 (Figure 4F, bar 3), the light-scattering intensity of pH 7.5-like fibrils increased to a level greater than that of pH 2.9 fibrils (Figure 4F, bar 2). After the double pH-jump, the light-scattering intensity of the fibrils slightly decreased (Figure 4F, bar 4), but remained larger than that before the pH-jump (Figure 4F, bar 2). These observations correspond to the EM observation that fibrils remained partially associated even after the double-pH jump (Figure 4C–E). In addition, all samples were centrifuged at 30,000 × g for 1 h, and the fractions of precipitated fibrils were estimated (Figure 4F, right ordinate). With the exception of H2 monomer (Figure 4F,

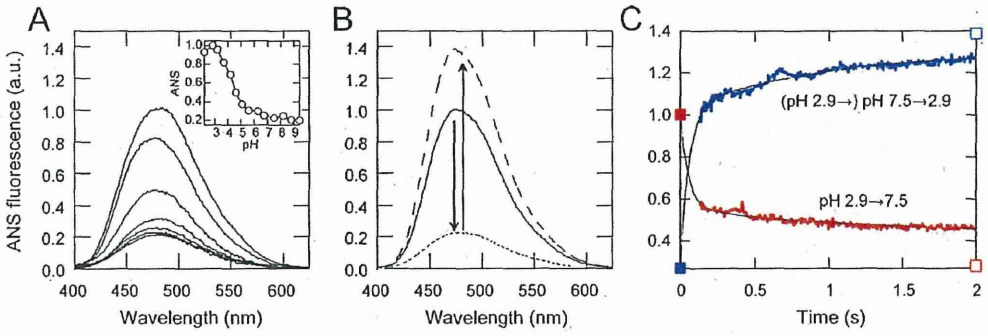

Figure 6. Conformational change of H2 fibrils monitored by ANS fluorescence stopped-flow. (A) Static ANS fluorescence spectra of the fibrils formed at various pHs. The solution pHs from top to bottom, at 475 nm are: pH 2.9, 3.7, 4.6, 5.6, 6.7, 7.5, and 8.8. The inset shows the ANS intensity at 475 nm as a function of pH. (B) H2 fibrils after a single pH-jump from 2.9 to 7.5 (dotted line) and a double pH-jump, pH 2.9 → 7.5 → 2.9, after incubation for 10 min at pH 7.5 (dashed line), and before the pH-jump of pH 2.9 fibrils (solid line) and pH 7.5 fibrils (gray solid line). (C) Kinetics of conformational changes of the H2 fibrils after a single pH-jump from 2.9 to 7.5 (red) and a double pH-jump, pH 2.9 → 7.5 → 2.9 (blue), after incubation for 10 min at pH 7.5. The intensities of the ANS fluorescence before and after the single pH-jump are shown by red closed and open squares, respectively, and before and after the double pH-jump are shown by blue closed and open squares, respectively.

circle 1), there was no large difference in the fractions of H2 fibrils (Figure 4F, circles 2–5). Thus, EM images roughly reflect the overall morphological features in the solutions.

Fibril Conformation Monitored by FT-IR Absorption Spectra. In order to characterize the secondary structure of H2 fibrils, FT-IR absorption spectra were measured in aqueous solution. The amide I band (1600–1700 cm^{-1}) is known to be a sensitive probe for determination of secondary structure.[40,41] The FT-IR spectrum of pH2.9 fibrils before the pH-jump revealed major bands corresponding to intermolecular β-sheet and β-turn conformations with bands at 1623 cm^{-1} and 1666 cm^{-1}, respectively (Figure 5A,D). After the pH-jump from 2.9 to 7.5, the FT-IR spectrum dramatically changed and showed an intermolecular β-sheet conformation with a band at 1625 cm^{-1}, and the band indicating a β-turn conformation was not seen at 1666 cm^{-1} but at 1676 and 1689 cm^{-1}, assigned to a turn/loop conformation (Figure 5A,D).[42] The difference spectrum showed an increase in random conformations, with a band at 1640–1655 cm^{-1}, and a decrease in intermolecular β-sheet conformations at around 1623 cm^{-1} (Figure 5A). Thus, it appears that the pH-jump causes the conformational change from pH 2.9 fibrils to pH 7.5-like fibrils by disrupting the highly ordered β-sheet and β-turn conformations, coupled with a decrease in CD ellipticity at 207 nm (Figure 1A).

The FT-IR spectrum of the pH 7.5-like fibrils was certainly distinct from that of the pH 7.5 fibrils formed at pH 7.5 (Figure 5B,E). The difference spectrum showed that pH 7.5-like fibrils were somewhat rich in β-sheet conformation, with a band at 1630–1640 cm^{-1}, and poor in turn/loop conformation, with band at approximately 1668 cm^{-1} (Figure 5B). It appears that the β-sheet hydrogen bonds of pH 2.9 fibrils remain partially intact even after the pH-jump to 7.5, which leads to the large negative CD ellipticity, unlike that of fibrils formed at pH 7.5 (Figure 1A).

After the double pH-jump, pH 2.9 → 7.5 → 2.9, the major bands corresponding to intermolecular β-sheet and β-turn conformations, with bands at 1624 cm^{-1} and 1664 cm^{-1}, respectively, are comparable with the bands of pH 2.9 fibrils before the pH-jump (Figure 5C,F). However, the difference spectrum showed a decrease in intermolecular β-sheet conformations and an increase in random conformations at approximately 1624 cm^{-1} and 1649 cm^{-1} (Figure 5C), respectively. This result suggests that although the pH 7.5-like fibrils revert to a conformation very similar to that of the pH 2.9 fibrils, even after the double pH-jump they are contaminated with some fraction of the pH 7.5-like fibrils, as shown by the EM observations (Figure 4C–E).

Kinetic Analyses of Conformational Changes of H2 Fibrils Using ANS Fluorescence Stopped-Flow. To monitor the conformational changes of H2 fibrils within the dead time of manual mixing, a stopped-flow instrument composed of a PEEK tube with a diameter of 1.0 mm and a Y-shaped mixer with a 0.75-mm-diameter channel was manufactured. The instrument was designed to create laminar flow and efficient mixing of the amyloid fibril solution, including large aggregates, without choking. First, the dead time of the stopped-flow was estimated using the quenching reaction of *N*-acetyl-L-tryptophane-amide (NATA) fluorescence by *N*-bromosuccinimide (NBS) (Figure S2 of the Supporting Information),[43,44] and a dead time of 130 ms was obtained. In addition, the refolding reaction of β-lactoglobulin (βLG) was examined using Trp fluorescence (Figure S3 of the Supporting Information). The end of a transient overshoot corresponding to the partially structured intermediate populated on the millisecond time scale[45] was observed.

Subsequently, the conformation of H2 fibrils formed at various pH values was examined using static fluorescence of 1-anilinonaphthalene-8-sulfonic acid (ANS). The fluorescence intensity of ANS bound to the fibrils gradually decreased as the pH value of the solution increased (Figure 6A), indicating that the hydrophobic region that is partially exposed to the solvent in the aggregate-like fibrils formed around neutral pH is smaller than that in the thin fibrils formed at acidic pHs. It appears that in aggregate-like fibrils the hydrophobic region is buried within the associated fibrils (Figure 2C).

Next, the conformational change of H2 fibrils induced by the pH-jump from 2.9 to 7.5 was examined. The ANS fluorescence dramatically decreased to a level similar to that of aggregate-like pH 7.5 fibrils (Figure 6B), following the conformational change from pH 2.9 fibrils to pH 7.5-like fibrils. After the double pH-jump, pH 2.9 → 7.5 → 2.9, the ANS fluorescence increased by 1.4-fold over that observed in the pH2.9 fibrils before the pH-jump (Figure 6B). Although the precise details are unknown, it appears that the H2 fibrils may partially disorder after the double pH-jump, exposing the much more hydrophobic domains to the solvent. However, the CD and FT-IR spectra

and EM observations showed that the conformation of pH 2.9 fibrils reverted almost completely, as described above. Then, the kinetic conformational changes of the H2 fibrils were examined by combining ANS fluorescence and stopped-flow. After the single pH-jump from 2.9 to 7.5, the conformational change of the fibrils was instantaneous and could not be monitored within the dead time of 130 ms (Figure 6C). We analyzed the experimental data according to the following kinetic formula:

$$f(t) = A_0 + A_1\exp(-k_1 t) + A_2\exp(-k_2 t) \quad (1)$$

Although its trace could not be completely fitted by a double exponential curve (eq 1), it appears that the apparent rate constant of the fast phase (k_1), which may consist of several phases, was larger than 18.3 ± 1.01 s^{-1} and that of slow phase (k_2) was 0.73 ± 0.03 s^{-1}. After restoration of the solution pH to 2.9, the conformation of the fibrils again changed readily (Figure 6C). The fluorescence intensity was fitted by a double exponential curve relatively well, and the apparent rate constants of the fast (k_{-1}) and slow (k_{-2}) phases, after the double pH-jump, were determined to be 17.6 ± 0.77 s^{-1} and 1.05 ± 0.04 s^{-1}, respectively. Intriguingly, the kinetic constants of the fast and slow phases were almost identical between the single and the double pH-jumps, implying similar conversion processes of the fibrils, such as lateral association or dissociation of the preformed fibrils. Collectively, amyloid fibrils can be readily and nearly reversibly converted between two distinct conformations separated by a low energy barrier.

DISCUSSION

Amyloidogenicity of Helix 2 Region of PrP. Recent studies indicate that the low pH solution is an ideal trigger of PrP^C to PrP^β conversion and PrP amyloid fibril formation.[27−29] The salt bridges of native PrP have been calculated and analyzed by quantum chemical calculations,[46] and the detailed biophysical characteristics and NMR studies of $PrP^C \rightarrow PrP^\beta$ conversion process have also been reported.[28] Recently, incorporating Wenxiang diagrams[29,47,48] further summarized their research based on the NMR, CD spectra, and dynamic light scattering data at the low pH environment found that some salt bridges and the hydrophobic interactions in the three helices of the prion proteins can affect the helical structural stability. These studies have provided insight into the prion misfolding and the mechanism of amyloid fibril formation. According to the experimental results[49,50] and recent Wenxiang diagram analysis,[29] the helical structure of H1 is much more stable than that of helices H2 and H3, and helix H3 is more stable than H2.[29,46] Therefore, unstable H2 helix should be more easily converted to H2 fibrils under acidic pH environment. In addition, after the disulfide bond of PrP is reduced, helix H2 is no longer stable and is partially unfolded in the PrP structural conversion.[51] This is why H2 peptide is selected to study the pH-jump induced conformational transition.

Conformation Change of H2 Fibrils was Induced by a Single pH-Jump. In general, it is considered that amyloid fibrils, which are highly ordered supramolecular complexes, are stiffer than most functional intracellular biological filaments,[21] and are rigid like a needle. X-ray microcrystallography has revealed that the amyloid fibrils are composed of a pair of β-sheets with the facing side chains interdigitated in a steric zipper and are extremely highly ordered.[20,52] However, after pH-jump from 2.9 to 7.5, H2 fibril conformation readily changed to a distinct one as revealed by CD and FT-IR spectra (Figures 1 and 5), and morphological conversion from thin pH 2.9 fibrils to thick pH 7.5-like fibrils occurred (Figure 2D,H). Recently, Kurouski et al. reported the pH-induced conformational changes in insulin fibrils were detected using vibrational circular dichroism and fluid-cell atomic force microscope,[16] and temperature-induced structural rearrangement has also been reported for MoPrP fibrils.[38]

In the high pressure experiment, amyloid fibrils of β_2-microglobulin showed the structural reorganization into more tightly packed ones,[53] implying that amyloid fibrils are not tightly packed and contain a large number of cavities at atmosphere. Thus, although amyloid fibrils seem to be rigid, mature amyloid fibrils may not represent the most thermodynamically stable state.[16,38,53] Amyloid fibrils are proposed to be determined predominantly by the hydrogen bond network in the extended intermolecular β-sheet architecture of the peptide backbones,[21] but the packing between the side-chains may not be optimized.[16,38,53] Hence, it is possible that interactions between the side-chains modulate fibril conformation when the pH of the solution changes. In addition, these conversions were completed within a few seconds (Figure 6C). The pH profile of the conversions was almost identical to that of fibril formation for the H2 peptide (Figure 1C), both of which significantly changed at approximately pH 5. Thus, it appears that the side-chains of the H2 peptide were substantially exposed to the solvent when the fibrils were formed, enabling the rapid conformational change of the fibrils.

Nearly Reversible Conformational Change of H2 Fibrils After a Double pH-Jump. Intriguingly, the conformation of pH 7.5-like fibrils reverted to a conformation very similar to that of pH 2.9 fibrils when the solution pH was restored from 7.5 to 2.9 (Figure 3A), and these conversions were completed rapidly (Figure 6C). EM observation showed that the thick laterally associated pH 7.5-like fibrils dissociated into the thin pH 2.9 fibrils (Figure 4A,B), induced by electric repulsion between fibrils that were stacked by hydrophobic interactions at pH 7.5. Notably, these phenomena may be particular to amyloid fibrils and may not be observed for random aggregates, and observation of these results will depend on partial maintenance of the conformation of pH 2.9 fibrils after the pH-jump to 7.5. The CD and FT-IR spectra showed that pH 7.5-like fibrils, prepared by the pH-jump from 2.9 to 7.5, were certainly distinct from fibrils formed at pH 7.5 (Figures 1A and 5E).

In general, globular monomeric proteins readily relax conformation depending on the conditions, but amyloid fibrils are supramolecular complexes whose global conformational changes may be hindered by hydrogen bonds and hydrophobic interactions between both sides of the molecules, unless the fibrils dissolve into monomers. The partial remaining hydrogen bond network in the intermolecular β-sheet of the backbones, which may act like a clasp, can allow rapid reversible conformational changes between pH 7.5 and 2.9 by decreasing the energy of transition between pH 7.5-like fibrils and pH 2.9 fibrils. Thus, its rate constant was comparable to that of globular monomer protein folding.[54,55] If the pattern of hydrogen bonds were completely altered by the pH-jump, more time would be required to return to either the initial conformation or the distinct conformation of amyloid fibrils. In contrast, the reversibility decreased as incubation time at pH 7.5 increased (Figure 3C), because the amyloid fibrils could

gradually become strongly associated with each other through hydrophobic interactions. Thus, conformational change of the fibrils is feasible before they form large aggregates.

Proposed Pathways of Conformational Changes of H2 Fibrils. The H2 peptide formed pH 2.9 fibrils and pH 7.5 fibrils at pH 2.9 and 7.5, respectively (Figure 7). Their

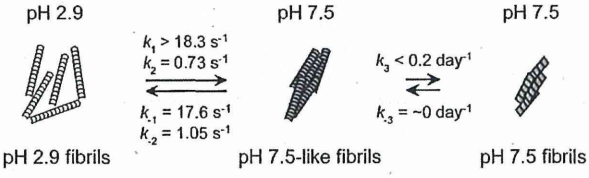

Figure 7. Proposed pathways of conformational changes of H2 fibrils. The H2 peptide formed pH 2.9 fibrils (left) and pH 7.5 fibrils (right) at pH 2.9 and 7.5, respectively. After the pH-jump from 2.9 to 7.5, pH 2.9 fibrils instantly changed to pH 7.5-like fibrils (middle), and reverted to pH 2.9 fibrils when the solution pH was restored to 2.9. The thick, laterally associated fibrils (middle) or aggregated fibrils (right) stacked by the hydrophobic interactions at pH 7.5 were painted gray.

conformations and morphologies are significantly different. After the pH-jump from 2.9 to 7.5, pH 2.9 fibrils instantly changed to pH 7.5-like fibrils, but pH 7.5-like fibrils partially retained the intermolecular hydrogen bonds of pH 2.9 fibrils. In addition, pH 7.5-like fibrils reverted to pH 2.9 fibrils when the solution pH was restored to 2.9 (Figure 7). Thus, the transition energy between pH 2.9 fibrils and pH 7.5-like fibrils is relatively low, and the relatively fast phases in the conversion between them were observed (0.7–18 s^{-1}). In contrast, the pH 7.5-like fibrils did not change to the pH 7.5 fibrils for at least 5 days (Figure 1D, inset), and pH 7.5 fibrils also did not change to pH 7.5-like fibrils even under identical conditions (data not shown), suggesting the presence of a high energy barrier between them (<0.2 day^{-1}) (Figure 7). To exceed these energy barriers, it might be necessary to break down the intermolecular restrictions in these fibrils completely.

These conformational changes of H2 fibrils were caused by the disruption of the balance between hydrophobic and electrostatic interactions resulting from the change in the solution pH, and thus the amyloid fibrils may have the potential to convert into distinct forms depending on the conditions. Theses conformational varieties of the amyloid fibrils may explain the physical background of the diversity in prion.

■ ASSOCIATED CONTENT

Supporting Information

Structure of MoPrP(121–231) and amino acid sequence of H2 peptide (MoPrP(172–194)), estimation of the dead-time of the stopped-flow instrument, and refolding of β-lactoglobulin (βLG) from the urea-denatured state at pH 3.0. This material is available free of charge via the Internet at http://pubs.acs.org.

■ AUTHOR INFORMATION

Corresponding Author

*Phone: +81 58 230 6145. E-mail: kuwata@gifu-u.ac.jp.

Funding

This work was supported by the Program for the Promotion of Fundamental Studies in Health Science of the National Institute of Biomedical Innovation, and by a grant from Research on Measures for Intractable Diseases (Prion Disease and Slow Virus Infections) of the Ministry of Health, Labour and Welfare of Japan. K. Yamaguchi was supported by the Japan Society for Promotion of Science (JSPS) Research Fellowship for Young Scientists. Y. O. Kamatari and K. Kuwata were supported by Grants-in-Aid for Scientific Research and X-ray Free Electron Laser (XFEL) program of the Ministry of Education, Culture, Sports, Science and Technology of Japan.

Notes

The authors declare no competing financial interest.

■ ACKNOWLEDGMENTS

We thank the Equipment Center for Common Research at the Graduate School of Medicine, Gifu University, for assistance with EM observations.

■ ABBREVIATIONS

ANS, 1-anilinonaphthalene-8-sulfonic acid; CD, circular dichroism; EM, electron microscope; FT-IR, Fourier transform infrared; H2 peptide, fragmented peptide of helix 2; MoPrP, mouse prion protein; PrP^C, cellular form of prion protein; PrP^{Sc}, scrapie form of prion protein; ThT, thioflavin T

■ REFERENCES

(1) Rochet, J. C., and Lansbury, P. T., Jr. (2000) Amyloid fibrillogenesis: themes and variations. *Curr. Opin. Struct. Biol. 10*, 60–68.

(2) Cohen, F. E., and Kelly, J. W. (2003) Therapeutic approaches to protein-misfolding diseases. *Nature 426*, 905–909.

(3) Prusiner, S. B. (1998) Prions. *Proc. Natl. Acad. Sci. U.S.A. 95*, 13363–13383.

(4) Uversky, V. N., and Fink, A. L. (2004) Conformational constraints for amyloid fibrillation: the importance of being unfolded. *Biochim. Biophys. Acta 1698*, 131–153.

(5) Collinge, J., Sidle, K. C. L., Meads, J., Ironside, J., and Hill, A. F. (1996) Molecular analysis of prion strain variation and the aetiology of 'new variant' CJD. *Nature 383*, 685–690.

(6) Bruce, M. E., Will, R. G., Ironside, J. W., McConnell, I., Drummond, D., Suttie, A., McCardle, L., Chree, A., Hope, J., Birkett, C., Cousens, S., Fraser, H., and Bostock, C. J. (1997) Transmissions to mice indicate that 'new variant' CJD is caused by the BSE agent. *Nature 389*, 498–501.

(7) Aguzzi, A., and Polymenidou, M. (2004) Mammalian prion biology: one century of evolving concepts. *Cell 116*, 313–327.

(8) Weissmann, C. (2004) The state of the prion. *Nat. Rev. Microbiol. 2*, 861–871.

(9) Riek, R., Hornemann, S., Wider, G., Billeter, M., Glockshuber, R., and Wuthrich, K. (1996) NMR structure of the mouse prion protein domain PrP(121–231). *Nature 382*, 180–182.

(10) Pan, K.-M., Baldwin, M., Nguyen, J., Gasset, M., Serban, A., Groth, D., Mehlhorn, I., Huang, Z., Fletterick, R. J., Cohen, F. E., and Prusiner, S. B. (1993) Conversion of α-helices into β-sheets features in the formation of the scrapie prion proteins. *Proc. Natl. Acad. Sci. U.S.A. 90*, 10962–10966.

(11) Collinge, J. (2001) Prion diseases of humans and animals: their causes and molecular basis. *Annu. Rev. Neurosci. 24*, 519–550.

(12) Jones, E. M., and Surewicz, W. K. (2005) Fibril conformation as the basis of species-and strain-dependent seeding specificity of mammalian prion amyloids. *Cell 121*, 63–72.

(13) Makarava, N., Ostapchenko, V. G., Savtchenko, R., and Baskakov, I. V. (2009) Conformational switching within individual amyloid fibrils. *J. Biol. Chem. 284*, 14386–14395.

(14) Ban, T., Yamaguchi, K., and Goto, Y. (2006) Direct observation of amyloid fibril growth, propagation, and adaptation. *Acc. Chem. Res. 39*, 663–670.

(15) Li, J., Browning, S., Mahal, S. P., Oelschlegel, A. M., and Weissmann, C. (2010) Darwinian evolution of prions in cell culture. *Science 327*, 869–872.
(16) Kurouski, D., Dukor, R. K., Lu, X., Nafie, L. A., and Lednev, I. K. (2012) Spontaneous inter-conversion of insulin fibril chirality. *Chem. Commun. 48*, 2837–2839.
(17) Van Melckebeke, H., Wasmer, C., Lange, A., Ab, E., Loquet, A., Böckmann, A., and Meier, B. H. (2010) Atomic-resolution three-dimensional structure of HET-s(218–289) amyloid fibrils by solid-state NMR spectroscopy. *J. Am. Chem. Soc. 132*, 13765–13775.
(18) Paravastu, A. K., Leapman, R. D., Yau, W.-M., and Tycko, R. (2008) Molecular structural basis for polymorphism in Alzheimer's β-amyloid fibrils. *Proc. Natl. Acad. Sci. U.S.A. 105*, 18349–18354.
(19) Iwata, K., Fujiwara, T., Matsuki, Y., Akutsu, H., Takahashi, S., Naiki, H., and Goto, Y. (2006) 3D structure of amyloid protofilaments of β_2-microglobulin fragment probed by solid-state NMR. *Proc. Natl. Acad. Sci. U.S.A. 103*, 18119–18124.
(20) Sawaya, M. R., Sambashivan, S., Nelson, R., Ivanova, M. I., Sievers, S. A., Apostol, M., Thompson, M. J., Balbirnie, M., Wiltzius, J. J. W., McFarlane, H. T., Madsen, A., Riekel, C., and Eisenberg, D. (2007) Atomic structures of amyloid cross-β spines reveal varied steric zippers. *Nature 447*, 453–457.
(21) Knowles, T. P., Fitzpatrick, A. W., Meehan, S., Mott, H. R., Vendruscolo, M., Dobson, C. M., and Welland, M. E. (2007) Role of intermolecular forces in defining material properties of protein nanofibrils. *Science 318*, 1900–1903.
(22) Kaylor, J., Bodner, N., Edridge, S., Yamin, G., Hong, D.-P., and Fink, A. L. (2005) Characterization of oligomeric intermediates in α-synuclein fibrillation: FRET studies of Y125W/Y133F/Y136F α-synuclein. *J. Mol. Biol. 353*, 357–372.
(23) Bitan, G., Kirkitadze, M. D., Lomakin, A., Vollers, S. S., Benedek, G. B., and Teplow, D. B. (2003) Amyloid β-protein (Aβ) assembly: Aβ40 and Aβ42 oligomerize through distinct pathways. *Proc. Natl. Acad. Sci. U.S.A. 100*, 330–335.
(24) Kyte, J., and Doolittle, R. F. (1982) A simple method for displaying the hydropathic character of a protein. *J. Mol. Biol. 157*, 105–132.
(25) Deléage, G., Combet, C., Blanchet, C., and Geourjon, C. (2001) ANTHEPROT: an integrated protein sequence analysis software with client/server capabilities. *Comput. Biol. Med. 31*, 259–267.
(26) Yamaguchi, K., Matsumoto, T., and Kuwata, K. (2008) Critical region for amyloid fibril formation of mouse prion protein: unusual amyloidgenic properties of the helix 2 peptide. *Biochemistry 47*, 13242–13251.
(27) Gerber, R., Tahiri-Alaoui, A., Hore, P. J., and James, W. (2008) Conformational pH dependence of intermediate states during oligomerization of the human prion protein. *Protein Sci. 17*, 537–544.
(28) Bjorndahl, T. C., Zhou, G. P., Liu, X., Perez-Pineiro, R., Semenchenko, V., Saleem, F., Acharya, S., Bujold, A., Sobsey, C. A., and Wishart, D. S. (2011) Detailed biophysical characterization of the acid-induced PrP(c) to PrP(β) conversion process. *Biochemistry 50*, 1162–1173.
(29) Zhou, G. P., and Huang, R. B. (2013) The pH-triggered conversion of the PrP^C to PrP^{Sc}. *Curr. Top. Med. Chem. 13*, 1152–1163.
(30) Weddell, W. J. (1956) A simple ultraviolet spectrophotometric method for the determination of protein. *J. Lab. Clin. Med. 48*, 311–314.
(31) Adachi, R., Yamaguchi, K., Yagi, H., Sakurai, K., Naiki, H., and Goto, Y. (2007) Flow-induced alignment of amyloid protofilaments revealed by linear dichroism. *J. Biol. Chem. 282*, 8978–8983.
(32) Saiki, M., Honda, S., Kawasaki, K., Zhou, D., Kaito, A., Konakahara, T., and Morii, H. (2005) Higher-order molecular packing in amyloid-like fibrils constructed with linear arrangements of hydrophobic and hydrogen-bonding site-chains. *J. Mol. Biol. 348*, 983–998.
(33) Hollósi, M., Kövér, K. E., Holly, S., Radics, L., and Fasman, G. D. (1987) β-Turns in bridged proline-containing cyclic peptide models. *Biopolymers 26*, 1555–1572.
(34) Gierasch, L. M., Deber, C. M., Madison, V., Niu, C. H., and Blout, E. R. (1981) Conformations of $(X\text{-}_L\text{-Pro-Y})_2$ cyclic hexapeptides. Preferred β-turn conformers and implications for β-turns in proteins. *Biochemistry 20*, 4730–4738.
(35) Rose, G. D., Gierasch, L. M., and Smith, J. A. (1985) Turns in peptides and proteins. *Adv. Protein Chem. 37*, 1–109.
(36) Fujii, T., Iwane, A. H., Yanagida, T., and Namba, K. (2010) Direct visualization of secondary structures of F-actin by electron cryomicroscopy. *Nature 467*, 724–728.
(37) Anfinsen, C. B. (1973) Principles that govern the folding of protein chains. *Science 181*, 223–230.
(38) Bocharova, O. V., Makarava, N., Breydo, L., Anderson, M., Salnikov, V. V., and Baskakov, I. V. (2006) Annealing prion protein amyloid fibrils at high temperature results in extension of a proteinase K-resistant core. *J. Biol. Chem. 281*, 2373–2379.
(39) Sabaté, R., Baxa, U., Benkemoun, L., Sánchez de Groot, N., Coulary-Salin, B., Maddelein, M. I., Malato, L., Ventura, S., Steven, A. C., and Saupe, S. J. (2007) Prion and non-prion amyloids of the HET-s prion forming domain. *J. Mol. Biol. 370*, 768–783.
(40) Barth, A., and Zscherp, C. (2002) What vibrations tell us about proteins. *Q. Rev. Biophys. 35*, 369–430.
(41) Seshadri, S., Khurana, R., and Fink, A. L. (1999) Fourier transform infrared spectroscopy in analysis of protein deposits. *Methods Enzymol. 309*, 559–576.
(42) Bandekar, J. (1992) Amide modes and protein conformation. *Biochim. Biophys. Acta 1120*, 123–143.
(43) Bilsel, O., Kayatekin, C., Wallace, L. A., and Matthews, C. R. (2005) A microchannel solution mixer for studying microsecond protein folding reactions. *Rev. Sci. Instrum. 76*, 014302.
(44) Peterman, B. F. (1979) Measurement of the dead time of a fluorescence stopped-flow instrument. *Anal. Biochem. 93*, 442–444.
(45) Kuwata, K., Shastry, R., Cheng, H., Hoshino, M., Batt, C. A., Goto, Y., and Roder, H. (2001) Structural and kinetic characterization of early folding events in β-lactoglobulin. *Nat. Struct. Biol. 8*, 151–155.
(46) Ishikawa, T., and Kuwata, K. (2010) Interaction analysis of the native structure of prion protein with quantum chemical calculations. *J. Chem. Theor. Comput. 6*, 538–547.
(47) Chou, K. C., Zhang, C. T., and Maggiora, G. M. (1997) Disposition of amphiphilic helices in heteropolar environments. *Proteins 28*, 99–108.
(48) Chou, K. C., Lin, W. Z., and Xiao, X. (2011) Wenxiang: a web-server for drawing wenxiang diagrams. *Nat. Sci. 3*, 862–865.
(49) DeMarco, M. L., and Daggett, V. (2007) Molecular mechanism for low pH triggered misfolding of the human prion protein. *Biochemistry 46*, 3045–3054.
(50) Ziegler, J., Sticht, H., Marx, U. C., Müller, W., Rösch, P., and Schwarzinger, S. (2003) CD and NMR studies of prion protein (PrP) helix 1. Novel implications for its role in the $PrP^C \rightarrow PrP^{Sc}$ conversion process. *J. Biol. Chem. 278*, 50175–50181.
(51) Sang, J. C., Lee, C.-Y., Luh, F. Y., Huang, Y.-W., Chiang, Y.-W., and Chen, R. P. (2012) Slow spontaneous α-to-β structural conversion in a non-denaturing neutral condition reveals the intrinsically disordered property of the disulfide-reduced recombinant mouse prion protein. *Prion 6*, 489–497.
(52) Nelson, R., Sawaya, M. R., Balbirnie, M., Madsen, A. Ø., Riekel, C., Grothe, R., and Eisenberg, D. (2005) Structure of the cross-β spine of amyloid-like fibrils. *Nature 435*, 773–778.
(53) Chatani, E., Kato, M., Kawai, T., Naiki, H., and Goto, Y. (2005) Main-chain dominated amyloid structures demonstrated by the effect of high pressure. *J. Mol. Biol. 352*, 941–951.
(54) Baker, D. (2000) A surprising simplicity to protein folding. *Nature 405*, 39–42.
(55) Kamagata, K., Arai, M., and Kuwajima, K. (2004) Unification of the folding mechanisms of non-two-state and two-state proteins. *J. Mol. Biol. 339*, 951–965.

Send Orders for Reprints to reprints@benthamscience.net

2432 *Current Topics in Medicinal Chemistry,* 2013, *13,* 2432-2440

Logical Design of Medical Chaperone for Prion Diseases

Kazuo Kuwata*

United Graduate School of Drug Discovery and Medical Information Sciences, Department of Gene and Development, Graduate School of Medicine, Gifu University, 1-1 Yanagido, Gifu 501-1194, Japan

Abstract: A strategy of logical drug design (LDD) and its application to prion diseases are reviewed. LDD is primarily based on the localizability of a hot spot which initiates structural instability in the target protein. It is also based on the regulability of the hot spot by small compounds, their designabilty by a computer, their organic synthesizability and the specificity of their functions once administered to the biological organisms. Unification of localizability, regulability, producibility and specificity is the central theme of LDD. Theoretical foundation of LDD based on quantum theories is initially outlined. The localizability using nuclear magnetic resonance (NMR), the regulability by a medical chaperone, the synthesizability, and the functional specificity accomplished thus far, are then described.

Keywords: Logical drug design, quantum chemistry, prion, hot spot, medical chaperone.

1. THEORETICAL FOUNDATION OF LDD

Can we regulate the conformational dynamics of biological macromolecules, such as proteins by using the compounds?

In order to address this question, a theoretical framework for the geometrical regulation of biological systems including macromolecules as well as macroscopic organs was developed [1].

In essence, according to the cohomology theory, algebraic objects can be embedded into geometrical spaces. Therefore quantum theory, which essentially deals with the non-commutative operators in Hilbert space, can be also mapped into the non-commutative geometrical objects, and vice versa.

Although biological organisms have evolved through the accumulation of random processes, we do not have any concrete representation for this geometry at this stage. However, accumulation of the evidences on the geometrical regulation of the biological macromolecules as well as the macroscopic membranous structures would uncover the structural groups and the eigenstructures of biological systems embedded in the non-commutative spaces [1].

2. QUANTUM CHEMICAL APPROACH

In order to construct the representation of molecular system in biological space, an original program has been developed, called "Parallelized ab initio calculation system based on the fragment molecular orbital method (FMO) (PAICS)"[2].

*Address correspondence to this author at the United Graduate School of Drug Discovery and Medical Information Sciences, Department of Gene and Development, Graduate School of Medicine, Gifu University, 1-1 Yanagido, Gifu 501-1194, Japan; Tel: 81-58-230-6143; Fax: 81-58-230-6144; Email: kuwata@gifu-u.ac.jp

The solvent interaction and intra-molecular interaction the native structure of prion protein (PrP) were initially examined. The influence due to the geometrical fluctuation w taken into account by performing calculations on forty d ferent conformations. The solvent interaction energies c tained from the calculations provided information about t hydrophilicity of the three α-helices in PrP. The roles of t charged residues in retaining the native structure of PrP w the calculated intra-molecular interaction energies were a examined. The analysis, focused on van der Waals inter tion, showed that the hydrophobic residues were import for the stability of the native structure. The identified patl genic mutations of prion diseases were related to the hyd phobic interactions [3]. It is crucial to take into account t influence of geometrical fluctuations on quantum chemi calculations [3]. Other FMO studies on prion were also pu lished [4, 5].

Density functional theory (DFT) was then applied to c scribe the prion toxicity. A peptide fragment of human pri protein, HuPrP(106-126), was reported to mimic the patl logical features underlying prion diseases. Although the a tual neurotoxic mechanism of HuPrP(106-126) was elu dated, several hypotheses were proposed based on the role copper. In this study, to understand the toxic function HuPrP(106-126) from a viewpoint of electrochemical co petence, redox properties of copper ion complexes were vestigated with four different binding motifs of a model HuPrP(106-126). It was found that the HuPrP(106-126) c rived models exhibited diverse redox activities that depenc on copper-binding conformations [6].

FMO was applied to drug design & its optimization, pecially to examine the molecular interactions between prion protein (PrP) and GN8, which is a potential curat agent for prion diseases as described in detail below. T counterpoise method was introduced into the FMO sche to eliminate the basis set superposition error and examir the influence of geometrical fluctuation on the interacti

1873-5249/13 $58.00+.00

energies, thereby enabling rigorous analysis of the molecular interaction between PrP and GN8. This analysis could provide information on key amino acid residues of PrP as well as key units of GN8 involved in the molecular interaction between two molecules (Fig. **1a** & **b**) [2].

To perform the geometrical optimization, and also molecular dynamical simulation in a quantum space, the energy gradient of a specific region in a large molecule were obtained. First, a partial energy gradient (PEG) based on the fragment molecular orbital (FMO) method was defined. The suitability of PEG was examined by performing geometry optimizations of model systems, and it was found that optimization with PEG could provide almost the same geometry obtained with the full FMO energy gradient. Calculations on real biomolecular systems were carried out; these calculations demonstrated a great advantage of PEG in computational effort [7].

Furthermore, a quantum mechanical/molecular mechanical (QM/MM) method combined with the ab initio fragment molecular orbital (FMO) method, i.e., the ab initio FM(QM/MM method was proposed. By connecting a molecul dynamics (MD) program AMBER with an FMO progra PAICS, an AMBER-PAICS interface (AP-IF) was impl mented. Using the AP-IF, three example applications we implemented: (a) a hydrogen fluoride and water molecul clusters, (b) an alanine dipeptide in aqueous solution, and (a prion protein GN8 complex. From these results, it is co firmed that the FMO-QM/MM method offers a good cor promise between chemical accuracy and computational co and enables us to obtain in ab initio quality the inter- ar intramolecular interaction energies between molecules residues in large molecular systems such as solution ar biomolecule, by using the dynamics-based interfragme interaction energy (IFIE) analysis [8].

3. ACCURATE EVALUATION OF FREE ENERGY

Fragment molecular orbital (FMO) calculations were pe formed for the two binding modes of hen egg-whi

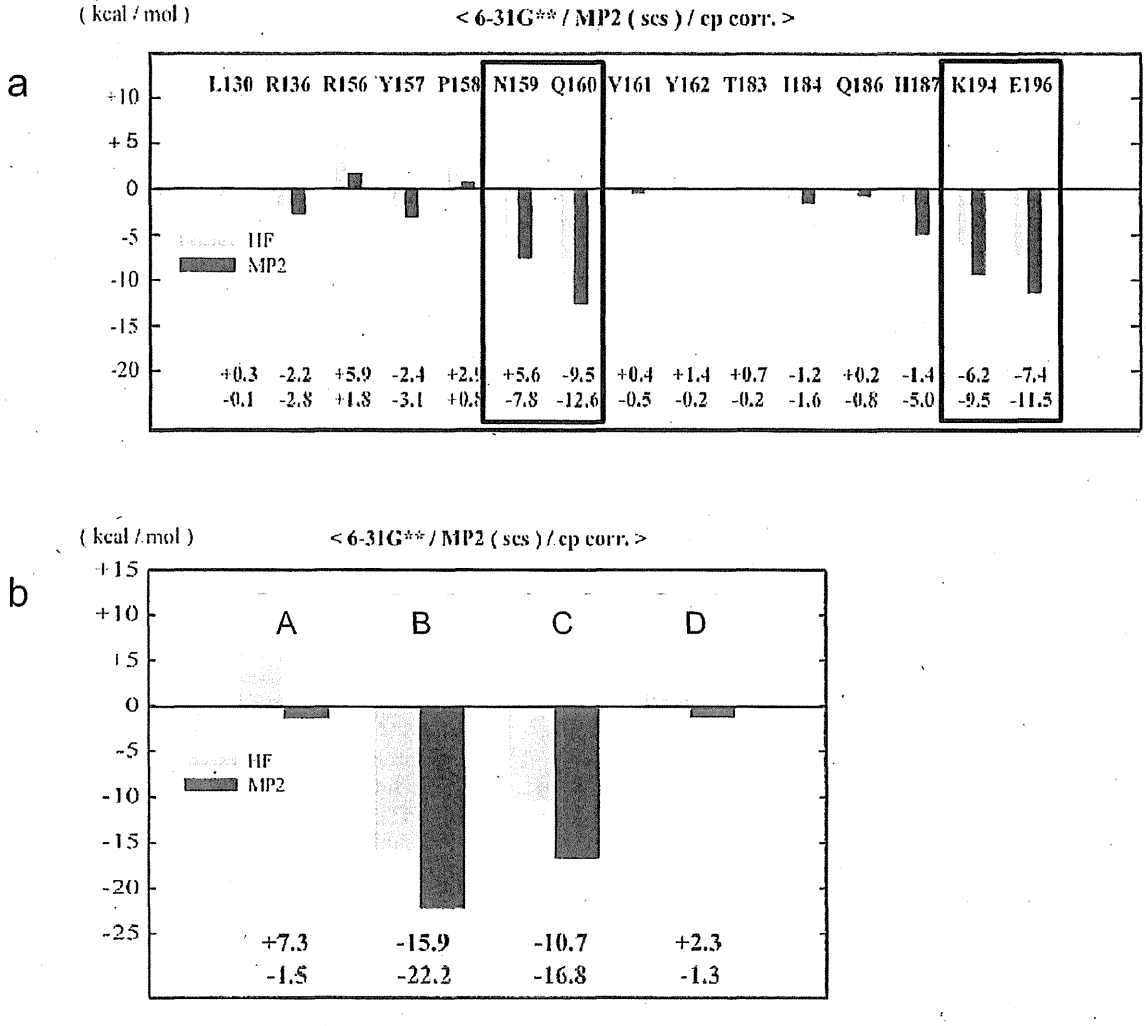

Fig. (1). (a) IFIE between amino acid residues in native prion protein. 6-31G**, MP2 (ses) and cp corr represent the basis set utilized, t Møller-Plesett method, and the counterpoise corrections, respectively. (**b**) IFIE between prion and GN8. GN8 was divided into four fra ments, A, B, C & D.

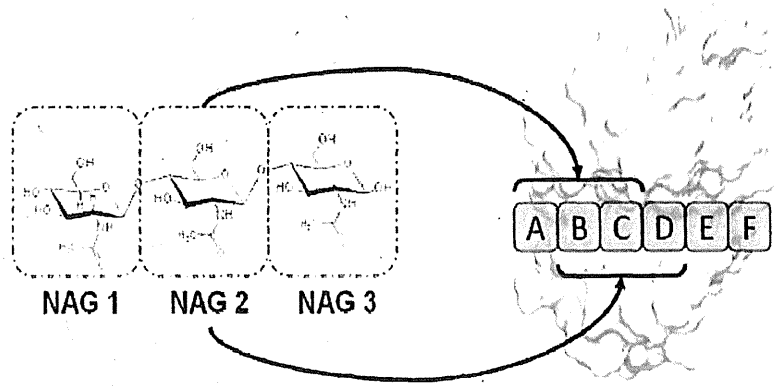

Fig. (2). NAG binding sites in lysozyme. TriNAG may bind to ABC mode 1 (x-ray analysis), BCD (mode 2), CDE, or DEF.

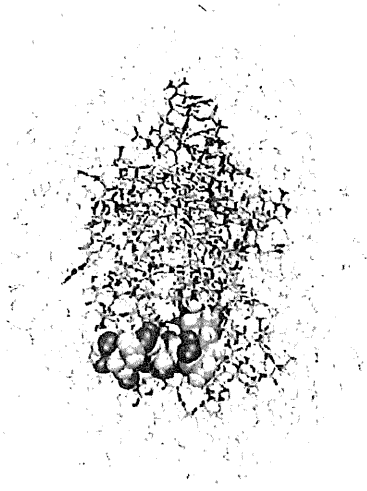

Fig. (3). A model structure of TriNAG-lysozyme complex surrounded by explicit water molecules. PAICS can calculate the wave-function of this large system within three days using a single CPU machine.

lysozyme with tri-N-acetyl-D-glucosamine (tri-NAG) (Fig. **2**), in order to examine its accuracy for predicting the interaction free energy. Solvent effects were considered using an explicit solvent model (Fig. **3**). For comparison with the computational results, the enthalpic contribution of the binding free-energy were experimentally determined (Figs. **4** & **5**). Calculations showed that the binding (mode 1 in Fig. **2**) observed by X-ray analysis was more stable than the other binding mode by -6.2 kcal mol^{-1} (Table **1**), where it was found that the interaction of protein with solvent molecules was crucial for this stability.

The amplitude of this energy difference was of the same order as the experimental enthalpic contribution. Detailed analysis using the energies divided into each residue was also consistent with a previous mutant study. In addition, the electron density analysis showed that the formal charge of the lysozyme (+8.0 e) was reduced to +5.16 e by charge transfer with solvent molecules [9]. The above calculations now construct the basis of LDD [10].

4. SELF-REPLICATION PROCESS OF A PRION

Since self-replication hypothesis of prion was propo [11], its real picture still have remained enigmatic. Althou many amyloids for neurodegeneration related peptides w reported [12], prion is essentially independent of amylc [13]. Then the propagation mechanism is a real questi how can oligomers self-replicate?

To construct a model of the propagation mechanism infectious scrapie-type prion protein (PrP^{Sc}), a disrupt simulation of a PrP^{Sc} nonamer using structure-based mole lar dynamics simulation method was conducted based o hypothetical PrP^{Sc} model structure [14]. The simulation sults showed that the nonamer disrupted in cooperative m ners into monomers via two significant intermediate sta (1) a nonamer with a partially unfolded surface trimer (2) a hexamer and three monomers. Dimers and trimers w rarely observed. Then, a new PrP^{Sc} propagation mechan was proposed where a hexamer plays an essential role a minimum infectious unit [15].

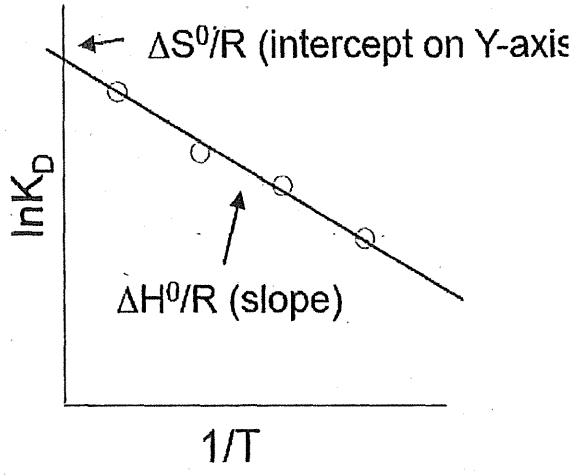

Fig. (4). Determination of ΔG, ΔH and ΔS using surface plas resonance (SPR) measurement. K_D values were obtained as a f tion of temperature. Slope and intercept correspond to the ent and enthalpy, respectively, in the plot of $R\ln(K_D)$ vs. 1/T.

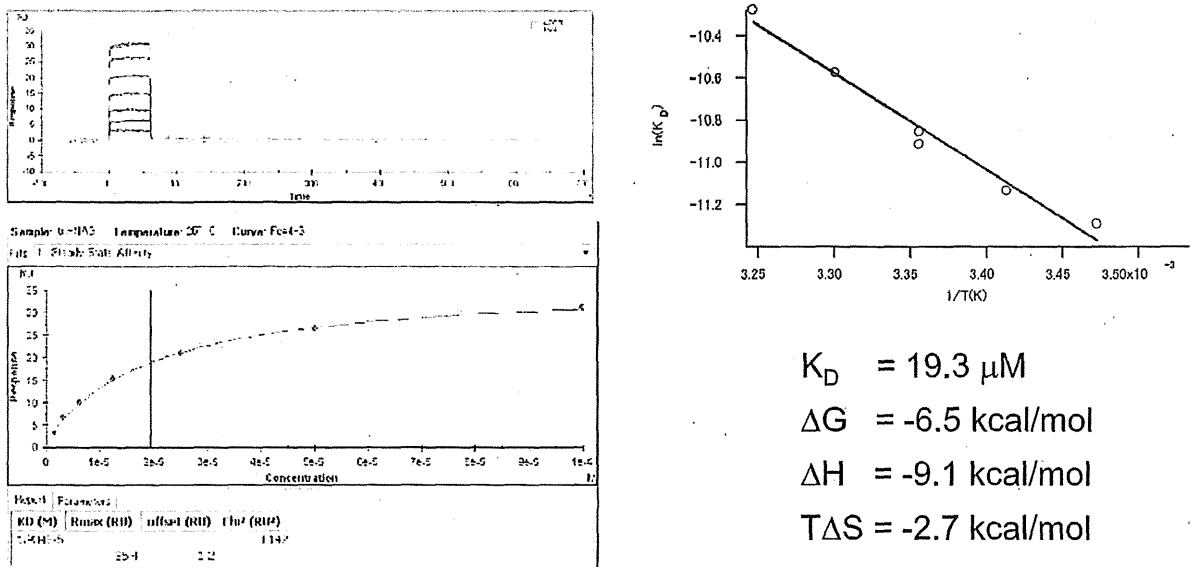

Fig. (5). Determination of ΔG, ΔH and ΔS for binding of TriNAG with lysozyme using surface plasmon resonance measurement. ΔG wa experimentally obtained to be -6.45 kcal/mol. , which is comparable to the value, -6.17 kcal/mol, which was predicted by quantum chemic calculation (see text and Table 1).

Table 1. Interaction Energy Obtained by PAICS

	Mode 1	Mode 2	Difference : 1 - 2
Protein internal energy	-32994793.62	-32994863.10	+69.48
Ligand internal energy	-1443674.35	-1443687.82	+13.47
Protein-solvent interaction energy	-6441.41	-6387.78	-53.63
Ligand-solvent interaction energy	-230.87	-209.58	-21.29
Protein –ligand interaction energy	-192.55	-178.38	-14.20

To gain insight into the structural mechanism of the conformational conversion process of prion, the potential amyloidogenic property of each secondary structural element in a mouse prion protein (mPrP) and their relative significance for the formation of amyloid fibrils were further experimentally examined [16]. Although peptides corresponding to α-helix 2 and α-helix 3 (named H2 peptide and H3 peptide, respectively) formed the amyloid-like fibrils, their structures were quite different. H2 fibrils formed the ordered β-sheet with the β-turn conformation, and the resultant fibrils were long and straight. In contrast, H3 fibrils consisted of the β-sheet with the random conformation, and the resultant fibrils were short and flexible. These properties are basically consistent with their hydrophobicity and β-strand propensity profiles. To examine the cross reactivity between peptide fragments and full-length mPrP, seeding experiments were carried out. While H2 seeds induced the formation of fibrils of full-length mPrP as quickly as full-length mPrP seeds, H3 seeds exhibited a long lag time. This implies that the region of α-helix 2 rather than α-helix 3 in mPrP has great potential for initiating fibril formation. As a whole, the α-helix 2 re gion would be crucial for the nucleation-dependent replica tion process of the prion protein [16].

The nucleation-dependent replication process of the prio protein is significantly enhanced by the ultrasonication [17 18]. Also it is known that the ultrasonication causes cavita tion in the solvent generating the special reaction file (Fig. 6) [19]. To elucidate the mechanisms of amyloid fibr formation under the ultrasonication, the ultrasonic powe using both calorimetry and potassium iodide (KI) oxidatio were quantitatively determined, and under the properly cali brated ultrasonic power, the ultasonication-induced amyloi formation process of the mouse prion protein (mPrP(23 231)) was investigated. These methods revealed that the ul trasonic power in the system ranged from 0.3 to 2.7 W bu entirely dependent on the positions of the ultrasonic stage Intriguingly, the nucleation time of the amyloid fibrils wa found to be shortened almost proportionally to the ultrasoni power, indicating that the probability of the occurrence o nucleus formation increases proportionally to the ultrasoni

power. Moreover, mPrP(23-231) formed two types of aggregates: rigid fibrils and short fibrils with disordered aggregates, depending on the ultrasonic power. The nucleation of rigid fibrils required an ultrasonic power larger than 1.5 W. While at the strong ultrasonic power larger than 2.6 W, amyloid fibrils were formed early, but simultaneously fine fragmentation of fibrils occurred. Thus, an ultrasonic power of approximately 2.0 W would be suitable for the formation of rigid mPrP(23231) fibrils under the conditions utilized (ultrasonication applied for 30 s every 9 min). As ultrasonication is widely used to amplify the scrapie form of the prion protein, or other amyloids *in vitro*, the calorimetry and KI oxidation methods proposed first might help determining the adequate ultrasonic powers necessary to amplify them efficiently [20].

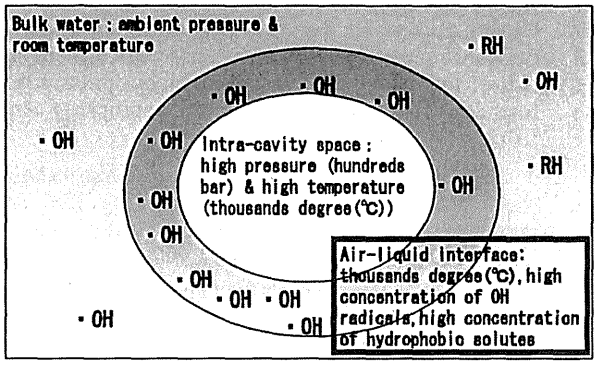

Fig. (6). An illustration of the cavitation reaction field. Under the ultrasonication, microscopic cavitation, i.e. formation of small bubble and its breakage, occurs more frequently in the solvent, than without sonication. When the bubble is broken, the intra-cavity pressure and temperature are transiently elevated upto several hundred bar and several thousand degree (°C), respectively, promoting the protein denaturation. At the air-water interface, $OH^{\cdot}$ radiclas are highly concentrated and may cause the modification of the covalent bonds at protein surface.

5. SCARCELY POPULATED HIGH-ENERGY STATE AND LEAD DISCOVERY

A crucial step for transformation of the normal cellular isoform of the prion protein (PrP^{C}) to the infectious prion protein (PrP^{Sc}) is thought to entail a previously uncharacterized intermediate conformer, PrP*, which interacts with a template PrP^{Sc} molecule in the conversion process [11]. By carrying out N^{15}-H^{1} two-dimensional NMR measurements under variable pressure on Syrian hamster prion protein rPrP(90-231), a metastable conformer of PrP^{C} coexisting at a population of similar to 1% at pH 5.2 and 30 °C was found, in which helices B and C are preferentially disordered. While the identity is still unproven, this observed metastable conformer is most logically PrP* or a closely related precursor. The structural characteristics of this metastable conformer are consistent with available immunological and pathological information about the prion protein [21].

Thermal stability was analyzed for the recombinant murine prion protein mPrP(23-231) with a single tryptophan mutation (F174W) and its perturbation by cold temperature. Compared to the N-terminally truncated ones, full-len construct is significantly unstable and forms intermedi state of urea denaturation, and also undergoes the cold des bilization under the ambient pressure. In order to detect very early phase of the folding, a laser-induced temperat jump kinetic measurement was applied and a kinetic ph of several microseconds was observed, suggesting the ba erless folding process. The conformational instability a low barriers between different conformers may explain unusual flexibility leading to the pathogenic conversion a the strain diversity [22].

In spite the mechanism of the conformational convers from the cellular (PrP^{C}) to the scrapie (PrP^{Sc}) form of anir prion proteins has yet to be elucidated, evidence is accun lating that may provide insight into the conversion proces atomic resolution. Critical aspects were shown for the sl fluctuation dynamics of the recombinant hamster prion p tein, rPrP(90-231), based on NMR relaxation analysis us Carr-Purcell-Meiboom-Gill (CPMG) experiments, and cc pare them in detail with results from high-pressure NM Residues exhibiting slow fluctuations on the time scale microseconds to milliseconds were mainly localized on h ces B and C (172-193 and 200-227), which include loc disordered regions in an intermediate conformer, PrP*, id tified previously by high-pressure NMR [21]. Moreo chemical shift differences between two putative exchang conformers obtained by the CPMG relaxation analysis the linear component of the pressure-induced chemical s changes were reasonably correlated at individual resi sites. These observations suggest that both the CMPG laxation and the pressure shifts reflect slow conformatic fluctuations and that these slow motions in PrP^{C} are rel to the trajectories leading to the transition to PrP* [23].

Although the precise mechanism of the conversion fi the cellular form (PrP^{C}) to the scrapie form (PrP^{Sc}) is unknown, a medical chaperone to stabilize the PrP^{C} con mation was discovered and the hot spots to stop the pat genic conversion was identified. In silico screening was ried out to find compounds that fitted into a "pocket" cre by residues undergoing the conformational rearrangem between the native and the sparsely populated high-ene states (PrP*) and that directly bind to those residues. Fo four selected compounds were tested in a TSE-infected culture model, among which one, 2-pyrrolidin-lyi-N-[4 (2-pyrrolidin-1-yl-acetylamino)-benzyl]-phenyl]-acetamic termed GN8, efficiently reduced PrP^{Sc}. Subsequently, ministration of GN8 was found to prolong the surviva TSE-infected mice. Heteronuclear NMR and comp simulation showed that the specific binding sites are the S2 loop (N159) and the region from helix B(V189,T192, K194) to B-C loop (E196), indicating that the intercala of these distant regions (hot spots) hampers the pathog conversion process. Logical drug design strategy focusin the hot spots of PrP^{c}, will open the way to the developn of novel anti-prion drugs [24].

6. A SYSTEMIC FLOW OF LOGICAL DRUG DESI

A flow of logical drug design, in contrast to the SE [25], is illustrated in Fig. 7 and also necessary items shown in Table 2.

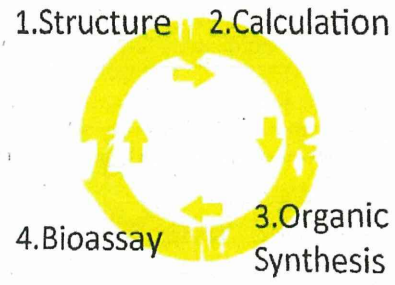

Fig. (7). A simplified flow of the logical drug design. Step 1. Structure and dynamics are determined using X-ray diffraction, NMR and/or cryo-electron microscopy. Step 2. Based on the structural dynamical information, appropriate ligands are logically designed using QC, AA and CG calculations. Step 3. The designed compounds are synthesized semi-automatically. Step 4. Synthesized compounds are subjected to the bioassays using the disease model cells or animals. If the compound are effective, the target-ligand complex structure is further analyzed and the process enters the recurrence cycle to step 2 and so on. It should be noted that the interfaces between steps have not been well developed. So one of the purpose of logical drug design is to construct the bridges between steps and unify all the necessary fields into an integrated scheme of logical drug design.

Table 2. Production System of Medical Chaperones

1	Individual genome information.
2	Target protein selection using network analysis.
3	Determination of structural dynamics (nuclear magnetic resonance (NMR), X-ray crystallography, electron microscopy (EM)).
4	Structural design and optimization of compounds (docking simulation (DS), fragment molecular orbital (FMO) methods, molecular dynamics simulation (MD), coarse grained (CG) model).
5	ADMET (absorption, distribution, metabolism, excretion, toxicity) prediction.
6	Determination of organic synthesis root.
7	Organic synthesis under the GMP (good manufacturing practice) regulation.
8	Preclinical examinations under the GLP (good laboratory practice) regulation (first in human).
9	ADME examination.
10	Clinical examinations under the GCP (good clinical practice) regulation.

Logical drug design is essentially an application of a non-commutative mathematical scheme [1], a general strategy of morphological regulation, which is applicable also to the surgical operation. As a representation of this theoretical framework, the quantum chemistry was used because it can describe the protein structural dynamics in aqueous solvent as well as the chemical reaction in organic solvent.

Structural dynamical & functional insight into the target protein is a prerequisite for the logical drug design. Then it is feasible to design the appropriate chemical structure of specific ligand for target using the above described comput tional approaches.

For organic synthesis of a designed molecule, there a pear some technical challenges, such as the robotic synthes and the GMP regulation. Then pharmacological characteriz tions, non-clinical safety examinations, and clinical tria follow. For orphan drugs, sometimes ultra-orphan, exhau tive governmental support would be required to commercia ize them because of the extremely small market size. It important to recognize that rare intractable diseases a sometimes fatal but anybody has a chance to get them.

Transmissible spongiform encephalopathy (TSE) inclu ing bovine spongiform encephalopathy (BSE), scrapie sheep, Creutzfeldt-Jakob disease in human, are transmitt by an isoform of a prion protein, and the conversion proce from the cellular conformation to the scrapie one (PrP^{Sc}) the key process for the regulation of the transmission pro ess. Since the reaction involves only non-covalent modific tion of the unique protein conformation, prion diseases a considered to be one of the most appropriate targets f LDD.

In fact, logical drug design is a general technique ar was already applied to anti-cancer drug [26] and ant influenza virus drug [27] discoveries. Notably a novel inhib tor with IC_{50} of 6 nM was found with potential anti-canc activity by the same technique [28].

7. CONCEPT OF MEDICAL CHAPERONE

Although some antiprion compounds were shown to i terfere with the pathological conversion of prion protein in a misfolded isoform, their actual mechanisms were not el cidated. Different conformations of prion protein with ar without ligand binding were compared, based on molecul dynamics simulations, to clarify the role of a typical ant prion compound termed GN8. Urea-driven unfolding simul tions were employed to assay whether or not GN8 preven denaturation of prion protein. It was found that urea mediat partial unfolding at helix B of the prion protein protein [29 suggesting a transition into the intermediate states of t pathological conversion. However, GN8 efficiently su pressed local fluctuations by binding to flexible spots c helix B and prevented its urea-induced denaturation. Thus was concluded that GN8 inhibits pathological conversion b suppressing the level of the intermediate. This is the fir evidence supporting the medical chaperone hypothesi which states that GN8 acts as a medical chaperone to stab lize the normal form of the prion protein. Although the proposed many kinds of chaperones as listed in Table **3**, t basic principle of 'medical chaperone' constitutes a promi ing strategy, i.e. thermodynamical stabilization of nati conformation, particularly for prion diseases as shown Fig. **8**, and possibly for other diseases related to protein mi folding [29].

Although a variety of antiprion compounds were reporte that are effective in *ex vivo* and *in vivo* treatment exper ments, the molecular mechanisms for most of these con pounds remain unknown. So antiprion mechanisms are cla sified into four categories: I, specific conformational stabil zation; II, nonspecific stabilization; III, aggregation; and I interaction with molecules other than PrP^C (Table **4**).

Table 3. Development of Chaperone Concept

	Name	Funcion
1	Chaperone	A class of proteins which prevent unwanted unfolding of other proteins by providing them with a proper environment for folding.
2	Medical chaperone	A class of small molecule which regulates the folding or dynamical processes of proteins or RNAs by binding t their specific sites (hot spots).
3	Chemical chaperone	A class of osmolytes such as glycerol and trehalose: they stabilize any protein nonspecifically.
4	Pharmaceutical chaperone	A class of small enzyme inhibitors that stabilize proteins by binding to them and prevent their degradation by t ubiquitin system.

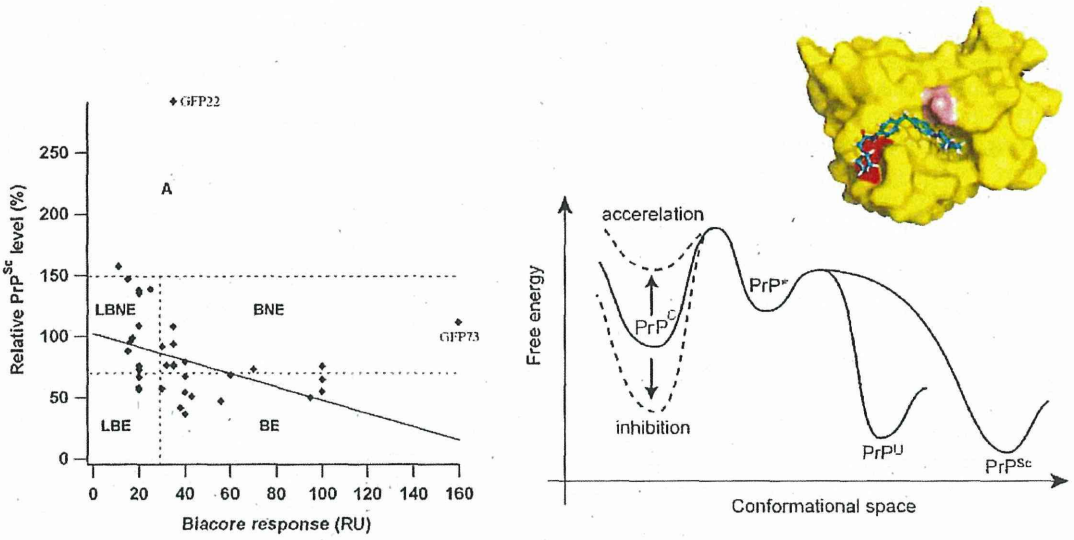

Fig. (8). The concept of medical chaperone. In general, a correlation between affinities and PrP^{Sc} inhibitory effects was observed for domly selected anti-prion compounds [34]. In principle, medical chaperone stabilizes the native conformation and increases the barrie tween the native conformation and the transition state (PrP*), thereby inhibiting the PrP^{Sc} generation.

Table 4. Classification of Anti-Prion Compounds

Class	Mechanism	Biacore	NMR
I	Specific conformational stabilization of PrP^C	Specific binding	Specific binding
II	Non-specific stabilization of PrP^C	Non-specific binding	Non-specific bindi
III	Aggregation and precipitaiton to reduce PrP^C population Aggregation and precipitaiton to reduce PrP population	Non-specific binding	Not detectable
IV	Interaction with molecules other than PrP^C	Non-specific binding	No interaction

To characterize antiprion compounds based on this classification, their binding affinities to PrP^C were determined using surface plasmon resonance and their binding sites on PrP^C using NMR spectroscopy. GN8 and GJP49 bound specifically to the hot spot in PrP^C, and acted as medical chaperones to stabilize the native conformation. Thus, mechanisms I was predominant. In contrast, quinacrine and epigallocathechin bound to PrP^C rather nonspecifically; these may stabilize the PrP^C conformation nonspecifically including the interference with the intermolecular interaction following mechanism II. Congo red and pentosan polysulfate bour PrP^C and caused aggregation and precipitation of PrP^C, reducing the effective concentration of prion protein. Tl fore, mechanism III was appropriate. Finally, CP-60, an rabone derivative, did not bind to PrP^C. Thus these classified into mechanism IV. However, their antiprior tivities were not confirmed in the GT + FK system, w details remain to be elucidated. This proposed anti mechanisms of diverse antiprion compounds could he elucidate their antiprion activities and facilitate effe

antiprion drug discovery [30]. In contrast, it was recently found that FK506 works as an anti-prion agent via mechanism IV , possibly the activation of the autophagy [31].

An RNA aptamer that tightly binds to and stabilizes PrP^C is expected to block this conversion and to thereby prevent prion diseases. It was shown that an RNA aptamer comprising only 12 residues, r(GGAGGAGGAGGA) (R12), reduces the PrP^{Sc} level in mouse neuronal cells persistently infected with the transmissible spongiform encephalopathy agent. Nuclear magnetic resonance analysis revealed that R12, folded into a unique quadruplex structure, forms a dimer and that each monomer simultaneously binds to two portions of the N-terminal half of PrP^C, resulting in tight binding. Electrostatic and stacking interactions contribute to the affinity of each portion. These results demonstrate the therapeutic potential of an RNA aptamer for to prion diseases [32]. The antiprion mechanism of the RNA aptamer may belong to mechanism I described above.

8. OPTIMIZATION OF CHEMICAL STRUCTURE

A series of GN8 derivatives were synthesized from various diamines, carboxylic acid derivatives, and nitrogen nucleophiles, and their antiprion activity was tested in TSE-infected mouse neuronal cells. It is found that two ethylenediamine units, hydrophobic substituents on the nitrogen atoms, and the diphenylmethane scaffold were essential structural features responsible for the activity. Seven derivatives bearing substituents at the benzylic position exhibited an improved antiprion activity with the IC_{50} values of 0.51-0.83 μM. Conformational analysis of model compounds suggested that the introduction of the substituent at the benzylic position restricted the conformational variability of the diphenylmethane unit [33].

CONCLUSION

Technical aspects of LDD have been almost established. Localizability of hot spot in prion protein was positively proved by nuclear magnetic resonance (NMR). Designability of medical chaperone was demonstrated using docking simulation, quantum chemical calculation, and molecular dynamics simulation. Synthesizability was also proved by synthesizing more than 200 derivatives. Regulability was also demonstrated by GT + FK system and *in vivo* treatment study. Specificity of medical chaperone is now examined under GMP and GLP regulations toward the first in human trial. Remaining themes for LDD would be the developments of the unified representation theory of medical chaperone and the unified tools to develop medical chaperones for various diseases.

To date we can connect the diseases and their possible therapeutics only empirically, since chemical structures of drugs themselves do not necessarily dictate their biological functions at current stage. However, carefully designed medical chaperone structures would well explain their biological functions through their specific interaction with the target proteins or nucleic acids.

In principle the concepts of LDD, i.e. localizability, designability, producibility, and specificity are general, and further applicable to the logical design of surgical operation devices such as the left ventricular assist device (LVAD [35] as a different class of medical chaperone.

CONFLICT OF INTEREST

The author(s) confirm that this article content has no conflicts of interest.

ACKNOWLEDGEMENTS

We thank Ms. Tomomi Saeki and Ms. Miku Yamada for technical help. We thank Professor Kurt Wüthrich and Dr. Simone Hornemann for kindly providing us with the expression plasmid of mouse PrP (121-231). We thank Ms. Miki Horii for the preparation of the recombinant proteins. K. K. was supported in part by a Grant-in-Aid for Scientific Research from the Ministry of Education, Culture, Sports, Science and Technology of Japan and Research on Measures for Intractable Diseases (Prion Disease and Slow Virus Infections from the Ministry of Health, Labour and Welfare. This study was supported by the Program for Promotion of Fundamental Studies in Health Science of the National Institute of Biomedical Innovation.

ABBREVIATIONS

LDD	=	Logical Drug Design
FMO	=	Fragment Molecular Orbital Method
PrP	=	Prion Protein
PEG	=	Partial Energy Gradient
QM	=	Quantum Mechanics
MM	=	Molecular Mechanics
MD	=	Molecular Dynamics
IFIE	=	Interfragment Interaction Energy
NAG	=	N-Acetyl-D-Glucosamine
SBDD	=	Structure Based Drug Design
CPMG	=	Carr-Purcell-Meiboom-Gill
NMR	=	Nuclear Magnetic Resonance
TSE	=	Transmissible Spongiform Encephalopathy
BSE	=	Bovine Spongiform Encephalopathy
LVAD	=	Left Ventricular Assist Device

REFERENCES

[1] Kuwata, K., Non-commutative Geometrical Drug Discovery - The Principle of Geometrical Regulation. *Yakugaku Zasshi-Journal of the Pharmaceutical Society of Japan,* **2012**, *132*, (8), 873-879.

[2] Ishikawa, T.; Ishikura, T.; Kuwata, K., Theoretical Study of the Prion Protein Based on the Fragment Molecular Orbital Method. *Journal of Computational Chemistry,* **2009**, *30*, (16), 2594-2601.

[3] Ishikawa, T.; Kuwata, K., Interaction Analysis of the Native Structure of Prion Protein with Quantum Chemical Calculations. *Journal of Chemical Theory and Computation,* **2010**, *6*, (2), 538-547.

[4] Hasegawa, K.; Mohri, S.; Yokoyama, T., Fragment molecular orbital calculations reveal that the E200K mutation markedly alters local structural stability in the human prion protein. *Prion,* **2010**, *4* (1), 38-44.

[5] Hasegawa, K.; Mohri, S.; Yokoyama, T., Comparison of the local structural stabilities of mammalian prion protein (PrP) by fragment molecular orbital calculations. *Prion,* **2013**, *7*, (2), 185-191.

[6] Yamamoto, N.; Kuwata, K., Difference in redox behaviors between copper-binding octarepeat and nonoctarepeat sites in prion protein. *Journal of Biological Inorganic Chemistry*, **2009**, *14*, (8), 1209-1218.

[7] Ishikawa, T.; Yamamoto, N.; Kuwata, K., Partial energy gradient based on the fragment molecular orbital method: Application to geometry optimization. *Chemical Physics Letters*, **2010**, *500*, (1-3), 149-154.

[8] Okamoto, T.; Ishikawa, T.; Koyano, Y.; Yamamoto, N.; Kuwata, K.; Nagaoka, M., A Minimal Implementation of the AMBER-PAICS Interface for Ab Initio FMO-QM/MM-MD Simulation. *Bulletin of the Chemical Society of Japan*, **2013**, *86*, (2), 210-222.

[9] Ishikawa, T.; Burri, R.R.; Kamatari, Y.O.; Sakuraba, S.; Matubayasi, N.; Kitao, A.; Kuwata, K., A theoretical study of the two binding modes between lysozyme and tri-NAG with an explicit solvent model based on the fragment molecular orbital method. *Physical Chemistry Chemical Physics*, **2013**, *15*, (10), 3646-3654.

[10] Kuwata, K.: Medical chaperone - A novel strategy for the Logical Drug Design. Drug Discovery & Therapy World Congress **2013**, Boston, IL16.

[11] Cohen, F.E.; Pan, K.M.; Huang, Z.; Baldwin, M.; Fletterick, R.J.; Prusiner, S.B., Structural clues to prion replication. *Science*, **1994**, *264*, (5158), 530-531.

[12] Shoji, M.; Golde, T.E.; Ghiso, J.; Cheung, T.T.; Estus, S.; Shaffer, L.M.; Cai, X.D.; McKay, D.M.; Tintner, R.; Frangione, B.; *et al.*, Production of the Alzheimer amyloid beta protein by normal proteolytic processing. *Science*, **1992**, *258*, (5079), 126-129.

[13] Prusiner, S.B., Cell biology. A unifying role for prions in neurodegenerative diseases. *Science*, **2012**, *336*, (6088), 1511-1513.

[14] Wille, H.; Michelitsch, M.D.; Guenebaut, V.; Supattapone, S.; Serban, A.; Cohen, F.E.; Agard, D.A.; Prusiner, S.B., Structural studies of the scrapie prion protein by electron crystallography. *Proc Natl Acad Sci U S A*, **2002**, *99*, (6), 3563-3568.

[15] Nakamura, H.K.; Takano, M.; Kuwata, K., Modeling of a propagation mechanism of infectious prion protein; a hexamer as the minimum infectious unit. *Biochemical and Biophysical Research Communications*, **2007**, *361*, (3), 789-793.

[16] Yamaguchi, K.I.; Matsumoto, T.; Kuwata, K., Critical Region for Amyloid Fibril Formation of Mouse Prion Protein: Unusual Amyloidogenic Properties of the Helix 2 Peptide. *Biochemistry*, **2008**, *47*, (50), 13242-13251.

[17] Saborio, G.P.; Permanne, B.; Soto, C., Sensitive detection of pathological prion protein by cyclic amplification of protein misfolding. *Nature*, **2001**, *411*, (6839), 810-813.

[18] Chatani, E.; Lee, Y.H.; Yagi, H.; Yoshimura, Y.; Naiki, H.; Goto, Y., Ultrasonication-dependent production and breakdown lead to minimum-sized amyloid fibrils. *Proc Natl Acad Sci U S A*, **2009**, *106*, (27), 11119-11124.

[19] Hasanzadeh, H.; Mokhtari-Dizaji, M.; Bathaie, S.Z.; Hassan, Z.M.; Nilchiani, V.; Goudarzi, H., Enhancement and control of acoustic cavitation yield by low-level dual frequency sonication: a subharmonic analysis. *Ultrason Sonochem*, **2011**, *18*, (1), 394-400.

[20] Yamaguchi, K.; Matsumoto, T.; Kuwata, K., Proper calibration of ultrasonic power enabled the quantitative analysis of the ultrasonication-induced amyloid formation process. *Protein Science*, **2012**, *21*, (1), 38-49.

[21] Kuwata, K.; Li, H.; Yamada, H.; Legname, G.; Prusiner, S.B.; Akasaka, K.; James, T.L., Locally disordered conformer of the hamster prion protein: A crucial intermediate to PrP[Sc]? *Biochemistry*, **2002**, *41*, (41), 12277-12283.

[22] Matsumoto, T.; Nakagawa, T.; Kuwata, K., Cold destabilizat and temperature jump of the murine prion protein mPrP(23-23 *Biochimica Et Biophysica Acta-Proteins and Proteomics*, **20** *1794*, (4), 669-673.

[23] Kuwata, K.; Kamatari, Y.O.; Akasaka, K.; James, T.L., Sl conformational dynamics in the hamster prion prot *Biochemistry*, **2004**, *43*, (15), 4439-4446.

[24] Kuwata, K.; Nishida, N.; Matsumoto, T.; Kamatari, Y. Hosokawa-Muto, J.; Kodama, K.; Nakamura, H.K.; Kimura, Kawasaki, M.; Takakura, Y.; Shirabe, S.; Takata, J.; Kataoka, Katamine, S., Hot spots in prion protein for pathogenic convers *Proceedings of the National Academy of Sciences of the Un States of America*, **2007**, *104*, (29), 11921-11926.

[25] Blundell, T.L., Structure-based drug design. *Nature*, **1996**, 3 (6604 Suppl), 23-26.

[26] Okuda, Y.; Nakamura, H.K.; Kuwata, K., Novel anti-car compounds: Structure-based discovery of chemical chaperons p53. *Oncology Reports*, **2009**, *22*, (4), 739-744.

[27] Fukuoka, M.; Minakuchi, M.; Kawaguchi, A.; Nagata, Kamatari, Y.O.; Kuwata, K., Structure-based discovery of a influenza virus A compounds among medicines. *Biochimica Biophysica Acta-General Subjects*, **2012**, *1820*, (2), 90-95.

[28] Endo, S.; Matsunaga, T.; Kuwata, K.; Zhao, H.T.; El-Kabbani, Kitade, Y.; Hara, A., Chromene-3-carboxamide derivat discovered from virtual screening as potent inhibitors of the tun maker, AKR1B10. *Bioorganic & Medicinal Chemistry*, **2010**, (7), 2485-2490.

[29] Yamamoto, N.; Kuwata, K., Regulating the Conformation of P. Protein through Ligand Binding. *Journal of Physical Chemistr* **2009**, *113*, (39), 12853-12856.

[30] Kamatari, Y.; Hayano, Y.; Yamaguchi, K.; Hosokawa-Muto Kuwata, K., Characterization of anti-prion compounds accordin the binding properties to the prion protein. *Protein Science*, **2** *21*, 154-154.

[31] Nakagaki, T.; Satoh, K.; Ishibashi, D.; Fuse, T.; Sano, Kamatari, Y.O.; Kuwata, K.; Shigematsu, K.; Iwamaru, Takenouchi, T.; Kitani, H.; Nishida, N.; Atarashi, R., FK reduces abnormal prion protein through the activation autolysosomal degradation and prolongs survival in prion-infe mice. *Autophagy*, **2013**, *9*, (9).

[32] Mashima, T.; Nishikawa, F.; Kamatari, Y.O.; Fujiwara, Saimura, M.; Nagata, T.; Kodaki, T.; Nishikawa, S.; Kuwata, Katahira, M., Anti-prion activity of an RNA aptamer and structural basis. *Nucleic Acids Research*, **2013**, *41*, (2), 1355-13

[33] Kimura, T.; Hosokawa-Muto, J.; Kamatari, Y.O.; Kuwata, Synthesis of GN8 derivatives and evaluation of their antip activity in TSE-infected cells. *Bioorganic & Medicinal Chem Letters*, **2011**, *21*, (5), 1502-1507.

[34] Hosokawa-Muto, J.; Kamatari, Y.O.; Nakamura, H.K.; Kuwata Variety of Antiprion Compounds Discovered through an In S Screen Based on Cellular-Form Prion Protein Struc Correlation between Antiprion Activity and Binding Affi *Antimicrobial Agents and Chemotherapy*, **2009**, *53*, (2), 765-77

[35] Slaughter, M.S.; Rogers, J.G.; Milano, C.A.; Russel, S.D.; C J.V.; Feldman, D; Sun, B.: Tatooles, A.J., Delgado,III,R.M.; L J.W.; Wozniak, T.C.; Ghumman, W.; Farrar, D.J.; Frazier C Advanced heart falure treated with cotinuous-flow left ventri assist device. *N. Engl. J. Med.* **2009**, *361*, (23), 2241-2284

Received: May 30, 2013 Revised: August 09, 2013 Accepted: August 22, 2013

ISSN 1348-2718

NEUROINFECTION

神経感染症

Vol. 18 No. 1 2013

日本神経感染症学会

Japanese Society for Neuroinfectious Diseases

〈シンポジウムⅠ〉プリオン病の最近の進歩

遺伝性プリオン病における病型と髄液所見

三條伸夫[1]、日熊麻耶[1]、北本哲之[2]、佐藤克也[3]、新竜一郎[3]、
西田教行[3]、山田正仁[4]、水澤英洋[1]

【要旨】本邦のプリオン病サーベイランス調査は1999年に開始され、これまでに353例(全体の18.6%)を遺伝性プリオン病と認定した。孤発性に比べて、遺伝性は表現型が多彩であり、*PRNP*変異における表現型の差が髄液に反映されているかどうかを確認するため、髄液バイオマーカーの14-3-3蛋白、tau蛋白を測定したところ、進行の早い表現型ほど高値になる傾向があり、神経細胞の変性の程度や速度を表していると考えられた。一方、QUIC法による髄液異常プリオン蛋白の定性所見が陽性の症例群は発症年齢が若く、罹病期間とは無関係だったことより、髄液異常プリオン蛋白は発症年齢に影響を与える因子である可能性が示唆された。

1. はじめに

本邦のプリオン病サーベイランス調査は1999年に開始され、2012年9月までに3,664名の患者のサーベイランス調査を行い、年2回のサーベイランス委員会を開催し、1,894例をプリオン病と認定した[1)]。そのうち遺伝性プリオン病は353例(18.6%)であった(図1)。遺伝性プリオン病のタイプ別頻度について、EUROCJDプロジェクト参加各国[2)]と本邦を比較すると、以前から指摘されているような欧米と日本の差というよりも、各国毎に異なっていると言った方が正確なのかもしれない(図2)。全プリオン病患者数に対する遺伝性プリオン病の比率は、EUROCJDではスロバキアの69.5%からスイスの1.2%まで幅広く分散しているが、平均は10.2%であるので、本邦の遺伝性プリオン病の比率は他国と比較して多いと考えられる[2)]。変異遺伝子別にみると、本邦ではプリオン蛋白遺伝子(PRNP)コドン180のValine(V)からIsoleucine(I)への変異であるV180Iのほか, M232R, P105Lなどの変異が認められていることが特徴的で、これらの変異は他の国ではほとんど報告がなく、言わば本邦特有の遺伝子変異であるといえる。コドン129や219などの正常多型以外の病的なPRNP異常はこれまでに、30種類以上の遺伝子変異と15種類の欠失・挿入が報告されている(図3)。遺伝性プリオン病は表現型により以下の様に分類できる。まず急速進行性CJDは古典型孤発型CJDと同様の経過をとり、E200KやM232Rの急速進行型がこれに相当する。次が緩徐進行型のCJDで急速進行型に比べると初期の進行が緩徐であるため、CJD以外の診断を受けていることがある。V180IやM232Rの緩徐進行型などがこれに相当する。そして、Gerstmann-Sträussler-Scheinker病(GSS)は小脳失調で発症し、緩徐に施行する。P102L症例のうち約8割の症例がこのタイプであり、P105Lは全例GSSになる。最後が致死性家族性不眠症(FFI)でコドン129の多型がMM型であるD187Nがこの病型を呈する。

孤発性プリオン病に比べて、遺伝性プリオン病は発症年齢、臨床病型、進行速度、予後などが各病型において大きく異なっている(表1)。そこで、表現型の差が髄液バイオマーカーに反映されているかどうか確認するため、本邦の遺伝性プリオン病における髄液バイオマーカーの14-3-3蛋白、tau蛋白の定量値、およびreal-time quaking-induced conversion (RT-QUIC)法[3)]による異常プリオン蛋白の定性所見と各病型の発症年齢、生存期間、症状の進行速度を比較検討した。

本邦の遺伝性プリオン病の特徴

本邦の遺伝性プリオン病の主な特徴は以下の2点

1：東京医科歯科大学大学院脳神経病態学（神経内科）
2：東北大学大学院プリオン病コアセンター
3：長崎大学医学部感染分子解析学
4：金沢大学大学院脳老化・神経病態学（神経内科）

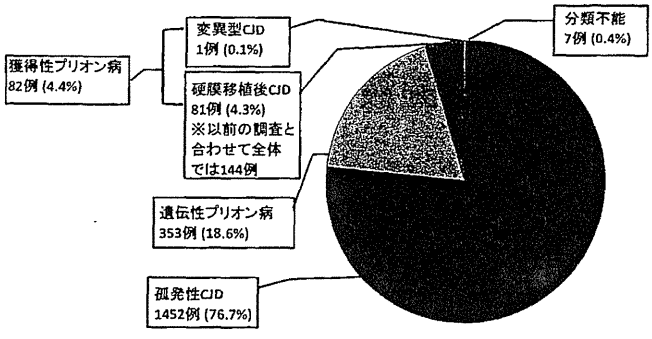

図1　本邦の遺伝性プリオン病の各病型患者数と頻度
1999年4月から2012年9月までのサーベイランス資料より作成

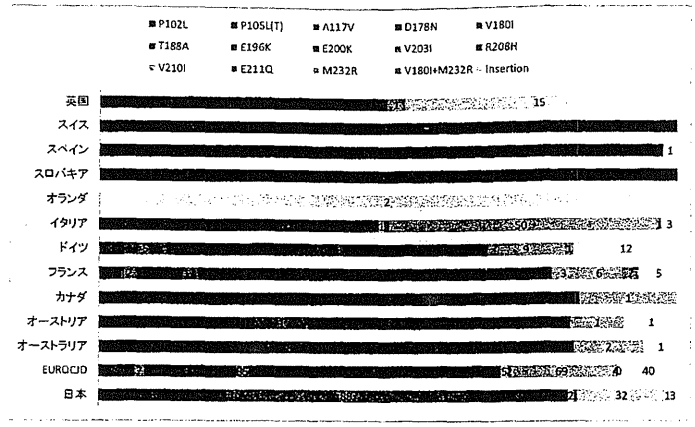

図2　各国別の遺伝性プリオン病における変異遺伝子毎の患者数と比率
EUROCJD参加11ヶ国と本邦の10年間のデータ同士で比較した。引用文献2より改変。本邦のデータは1999年4月から2009年3月までの10年間のサーベイランス資料より作成。

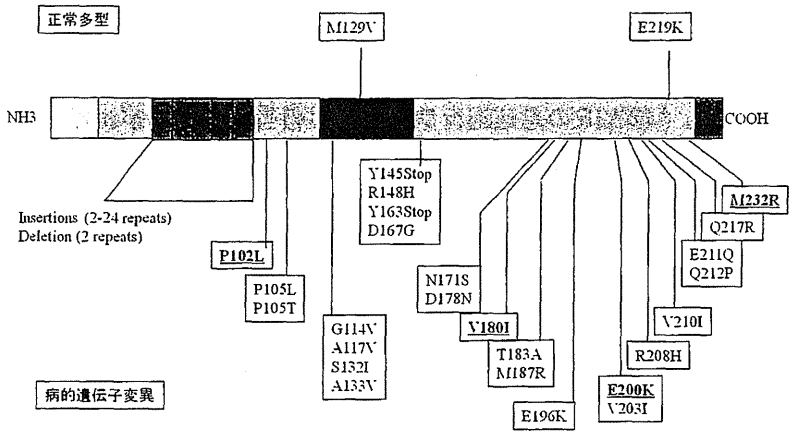

図3　プリオン蛋白遺伝子の正常多型と病的変異
上段が正常多型で下段が報告されている病的遺伝子変異を表している。プリオン蛋白は254のアミノ酸からなる蛋白で、カルボキシル末端にあるGPIアンカーを介して形質膜に結合している。本邦で多く認められる変異を下線で示した。

変異	P102L	P105L	D178N	V180I	E200K	V203I	R208H	V210I	M232R	V180I M232R	Insertion	その他
例数	57	8	4	151	46	3	1	1	50	1	3	6
%	13.40%	2.40%	1.90%	44.9%	13.7%	0.90%	0.50%	0.50%	14.0%	0.50%	1.40%	2.60%
発症年齢	55.2	44.3	57.8	76.5	58.6	73.0	74.0	55	63.9	73.0	49.7	
罹病期間（年）	4.5	11.0	1.2	1.9	1.1	0.8	2.8	0.2	1.7	2.3	2.1	
ミオクローヌス	31.40%	20.00%	75.00%	48.10%	88.60%	100%	100%		86.70%	100%	33.30%	
PSD	22.60%	0%	0%	11.60%	91.70%	100%	100%		64.50%	0%	66.70%	
MRI (DWI)	37.50%	0%	0%	100% *	93.80%	100%	100%		86.20%	100%	50.00%	
129MM	28	0	3	65	34	2	1	1	29	1	2	1
129MV	3	4	1	20	0	0	0	0	2	0	0	0

表1　各PRNP変異における表現型
1999年4月から2009年3月までの10年間のサーベイランス資料より作成

である。1つ目は上述したように、本邦特有のタイプがあるということで、以下の3つの変異が知られている。P105Lは本邦で6家系が報告されており[4]、若年で発症し、非常に緩徐な進行を呈する。認知機能障害の頻度は少なく、精神症状に先行して、失調症状や痙性対麻痺、末梢神経障害などを呈することより、P102Lと同様に脊髄小脳変性症の診断を受けていることがある。変異遺伝子がコドン129のバリンのアレル側にのみ認められる。本邦以外では、P105T(5)やP105S(6)の報告があるが、P105Lは本邦のみである。

V180Iは本邦の遺伝性プリオン病のうち約半数を占めている(図2)。記銘力障害で発症することが多いタイプで、初期の進行が緩徐であり家族歴をほとんど有していないことよりアルツハイマー型認知症と診断されていることもある[7]。本邦以外ではフランスと韓国[8]で報告されている。男女比が1:2で女性に多く、診断には脳MRIが有用であり、拡散強調画像(DWI)ではほぼ全例に後頭葉と中心溝前後を除いた全域に大脳皮質にリボン状、基底核に左右差のある高信号と、大脳皮質全体が浮腫状に腫脹する像を呈する(図4)[9]。

M232Rは古典型孤発性CJDと類似する急速進行例とMM2皮質型様の緩徐進行例が報告されており[10]、家族歴のある症例の報告がなく臨床上の特徴も乏しいため、原因遺伝子ではなく、リスク多型の可能性が指摘されている。診断のためには遺伝子検索が必須である。

逆に欧米ではE200Kについで多いV210Iは、本邦では2例のみ確認されており、頻度が少ない。

特徴の2番目は家族歴を有する症例が少ない点である。上述のようにV180IやM232Rでは家族歴のある症例がほとんどみられず、家族歴のある変異においても同一家系内で同一遺伝子変異が確認されているのはわずかに10.2%にとどまっている。これまでに浸透率に関する調査研究はされていないため、これらの変異が病的なものかリスク多型であるかは結論が出ていないが、V180Iに関しては特徴的な臨床症状から病因遺伝子である可能性が高いと思われる。

発症年齢と罹病期間の関係

各変異遺伝子の発症年齢と罹病期間の分布を図5上段に示した。特に目立つのはP105Lの症例では発症年齢が平均44.3と非常に若く、罹病期間が平均11年以上と非常に長いことで、対照的に、発症年齢が76.5と最も遅いV180Iは、罹病期間が1.9年と古典型孤発例に比べると長いが、それでも数ヶ月の差であり、このような臨床病型の差がどのような病的なプロセスの違いにより惹き起こされているのかわかっていない。発症年齢と罹病期間の相関解析を行うと、若年発症例ほど罹病期間が長い傾向があり、これは他の遺伝性疾患ではあまり認められない。

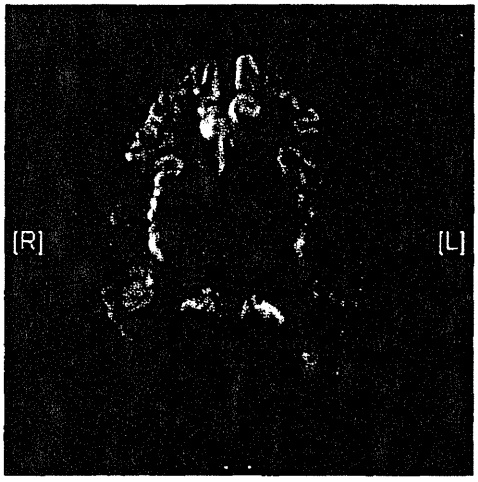

図4　V180I変異による遺伝性CJDの脳MRI拡散強調画像

遺伝性プリオン病の髄液中バイオマーカーの測定

遺伝性プリオン病の症例において、標準化ウエスタン・ブロット法による14-3-3蛋白、ELISA法による総tau蛋白という2種類のバイオマーカーの測定をおこなった。解析したのは*PRNP*変異がP102L、P105L、V180I、E200K、M232Rの症例で、髄液バイオマーカーの陽性率を図5下段に示した。各バイオマーカーは、進行の早い表現型で高値になる傾向があり、いずれのバイオマーカーも罹病期間が最も短いE200Kが最も高値であった。このことより、これらのバイオマーカーは神経細胞の障害(破壊)に伴って髄液中に放出されており、疾患の進行速度の早さや変性病変の強さを反映しているものと推測される。

一方、RT-QUIC法による髄液中の異常プリオン蛋白の検出率は、P102L、E200K、M232Rなどで80%を超えている一方、P105LやV180Iで陽性率が半分以下であるなど、臨床病型や病勢とは関連性が認められなかった(図6上段)。興味深いことに、RT-QUIC法が陽性の症例群では発症年齢が若く、RT-QUICの所見は罹病期間とは関連性が見いだせなかったこと(図6下段)より、髄液中の異常プリオ

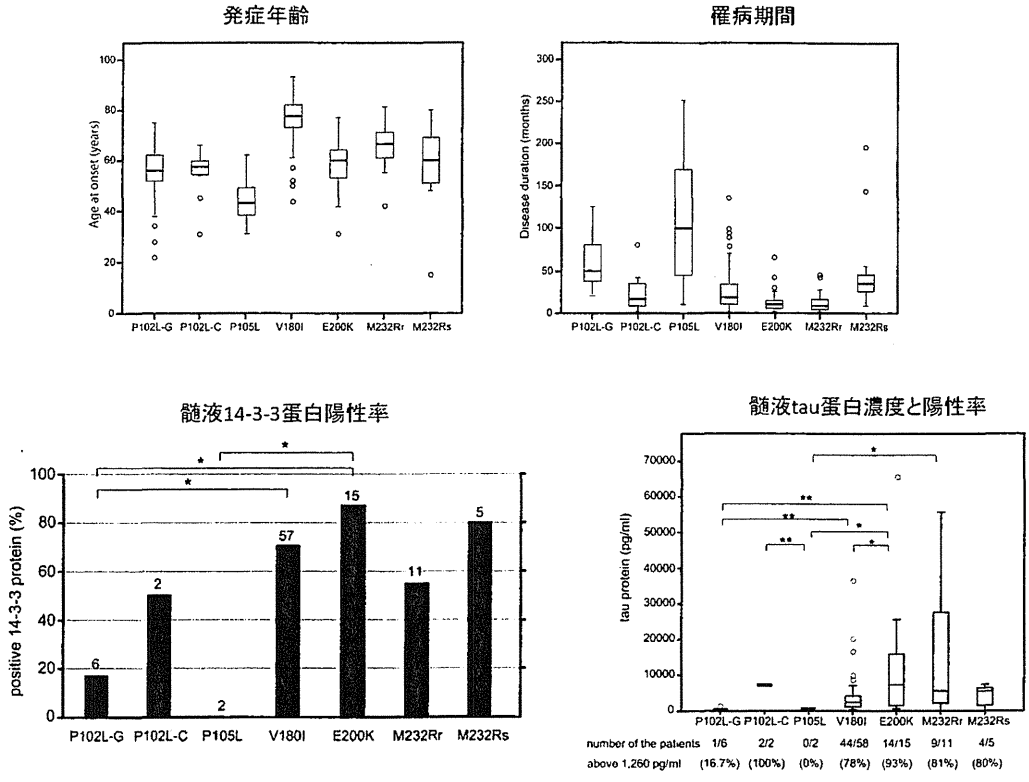

図5　各PRNP変異遺伝子における発症年齢(上段左)、罹病期間(上段右)、
髄液14-3-3(下段左)、髄液tau蛋白(下段右)

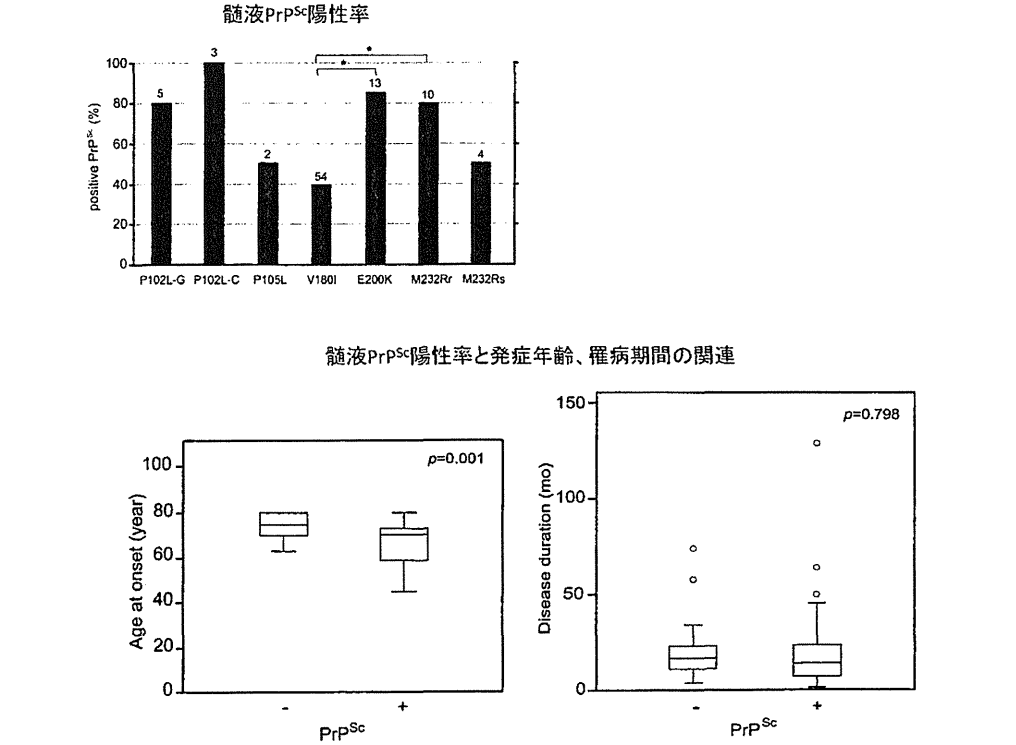

図6　各PRNP`変異における髄液異常プリオン蛋白(上段)と
発症年齢、罹病期間との関連(下段)

ン蛋白は発症年齢に影響を与える因子である可能性が示唆される。剖検脳における病理所見ではRT-QUIC陽性率が低いV180Iにおいて脳に沈着するプリオン蛋白は免疫染色、ウエスタン・ブロッティング共に弱陽性になるが、剖検脳における海綿状変化は非常に強いことが報告されており[11]、脳に沈着する異常プリオン蛋白の量や髄液中の異常プリオン蛋白と、神経変性の進行度は相関しない可能性があると思われた。このことは異常蛋白の蓄積から神経細胞変性までの過程において、防御する因子や調整する因子が存在することを示唆していると考えられ、そのような因子が解明できれば、プリオン病を含めたコンフォメーション病の治療法のヒントが得られるかもしれない。

謝辞

本サーベイランスにご協力いただきました患者様、およびご家族の方々、主治医の先生方に心からお礼申し上げます。本研究にご協力いただいておりますプリオン病サーベイランス委員の皆様に深謝いたします。

文献

1) Nozaki I, Hamaguchi T, Sanjo N, et al.: Prospective 10-year surveillance of human prion diseases in Japan. Brain 133(10): 3043-3057, 2010
2) Kovacs GG, Puopolo M, Ladogana A, et al.: Genetic prion disease: the EUROCJD experience. Hum Genet 118(2): 166-174, 2005
3) Atarashi R, Satoh K, Sano K, et al.: Ultrasensitive human prion detection in cerebrospinal fluid by real-time quaking-induced conversion. Nat Med 17(2): 175-178, 2011
4) Iwasaki Y, Kizawa M, Hori N, et al.: A case of Gerstmann-Straussler-Scheinker syndrome with the P105L prion protein gene mutation presenting with ataxia and extrapyramidal signs without spastic paraparesis. Clin Neurol Neurosurg 111(7): 606-609, 2009
5) Rogaeva E, Zadikoff C, Ponesse J, et al.: Childhood onset in familial prion disease with a novel mutation in the PRNP gene. Arch Neurol 63(7): 1016-1021, 2006
6) Tunnell E, Wollman R, Mallik S, et al.: A novel *PRNP*-P105S mutation associated with atypical prion disease and a rare PrPSc conformation. Neurology 71(18): 1431-1438, 2008
7) Jin K, Shiga Y, Shibuya S, et al.: Clinical features of Creutzfeldt-Jakob disease with V180I mutation. Neurology 62(3): 502-505, 2004
8) Yang TI, Jung DS, Ahn BY, et al.: Familial Creutzfeldt-Jakob disease with V180I mutation. J Korean Med Sci 25(7): 1097-1100, 2010
9) Ishida S, Sugino M, Koizumi N, et al.: Serial MRI in early Creutzfeldt-Jacob disease with a point mutation of prion protein at codon 180. Neuroradiology 37(7): 531-534, 1995
10) Shiga Y, Satoh K, Kitamoto T, et al.: Two different clinical phenotypes of Creutzfeldt-Jakob disease with a M232R substitution. J Neurol, 2007
11) Iwasaki Y, Mori K, Ito M, et al.: An autopsied case of V180I Creutzfeldt-Jakob disease presenting with panencephalopathic-type pathology and a characteristic prion protein type. Neuropathology 31(5): 540-548, 2011